Multi-model study of HTAP II on sulphur and nitrogen deposition

Jiani Tan[1], Joshua S. Fu[1], Frank Dentener[2], Jian Sun[1], Louisa Emmons[3], Simone Tilmes[3], Kengo Sudo[4], Johannes Flemming[5], Jan Eiof Jonson[6], Sylvie Gravel[7], Huisheng Bian[8], Yanko Davila[9], Daven K. Henze[9], Marianne T Lund[10], Tom Kucsera[11], Toshihiko Takemura[12], Terry Keating[13]

[1] Department of Civil and Environmental Engineering, University of Tennessee, Knoxville, TN, USA
[2] European Commission, Institute for Environment and Sustainability Joint Research Centre, Ispra, Italy
[3] Atmospheric Chemistry Observations and Modeling Laboratory, National Center for Atmospheric Research, Boulder, Colorado, USA
[4] Nagoya University, Furo-cho, Chikusa-ku, Nagoya, Japan
[5] European Centre for Medium-Range Weather Forecasts, Reading, UK
[6] Norwegian Meteorological Institute, Oslo, Norway
[7] Meteorological Research Branch, Meteorological Service of Canada, Toronto, Canada
[8] National Aeronautics and Space Administration Goddard Space Flight Center, Greenbelt, MD, USA
[9] Department of Mechanical Engineering, University of Colorado, Boulder, CO, USA
[10] CICERO Center for International Climate Research, Oslo, Norway
[11] Universities Space Research Association, NASA/GESTAR, Columbia, MD, USA
[12] Research Institute for Applied Mechanics, Kyushu University, Fukuoka, Japan
[13] US Environmental Protection Agency, Washington, DC, USA

Correspondence to: Joshua S. Fu (jsfu@utk.edu)

Abstract. This study uses multi-model ensemble results of 11 models from the 2nd phase of Task Force Hemispheric Transport of Air Pollution (HTAP II) to calculate the global sulfur (S) and nitrogen (N) deposition in 2010. Modelled wet deposition is evaluated with observation networks in North America, Europe and Asia. The modelled results agree well with observations, with 76-83% of stations having predicted within ±50% of observations. The results underestimate SO_4^{2-}, NO_3^- and NH_4^+ wet depositions in some European and East Asian stations, but overestimate NO_3^- wet deposition in Eastern United States. Inter-comparison with previous projects (PhotoComp, ACCMIP and HTAP I) shows HTPA II has considerably improved the estimation of deposition at European and East Asian stations. Modelled dry deposition is generally higher than the "inferential" data calculated by observed concentration and modelled velocity in North America, but the inferential data has high uncertainty, too. The global S deposition is 84 Tg(S) in 2010, with 49% of the deposits on continental regions and 51% on ocean (19% on coastal). The

global N deposition consists of 59 Tg(N) oxidized nitrogen (NO_y) deposition and 64 Tg(N) reduced nitrogen (NH_x) deposition in 2010. 65% of N is deposited on the continental regions and 35% is on ocean (15% on coastal). The estimated outflow of pollution from land to ocean is about 4 Tg(S) for S deposition and 18 Tg(N) for N deposition. Compared our results to the results in 2001 from HTAP I, we find that the global distributions of S and N depositions have changed considerably during the last 10 years. The global S deposition decreases 2 Tg(S) (3%) from 2001 to 2010, with significant decreases in Europe (5 Tg(S) and 55%), North America (3 Tg(S) and 29%) and Russia (2 Tg(S) and 26%), and increases in South Asia (2 Tg(S) and 42%) and the Middle East (1 Tg(S) and 44%). The global N deposition increases by 7 Tg(N) (6%), mainly contributed by South Asia (5 Tg(N) and 39%), East Asia (4 Tg(N) and 21%) and Southeast Asia (2 Tg(N) and 21%). The NH_x deposition is increased with no control policy on NH_3 emission in North America. On the other hand, NO_y deposition starts to dominate in East Asia (especially China) due to boosted NO_x emission.

1 Introduction

The nitrogen (N) plays an important role in the balance of the global ecosystem. Human activities such as consumption of fossil fuels, production and usage of N fertilizers and livestock cultivation disturb the N cycle in the ecosystem (Vitousek et al., 1997; Galloway et al., 2008). Estimation under the IPCC SRES A2 scenario predicts that the N deposition over land will increase by a factor of ~2.5 from 2000 to 2100 (Lamarque et al., 2005). Elevated N deposition can cause exceedance of N critical loads on ecosystems (Sanderson et al., 2006; Sun et al., 2017). 11% of the world's natural vegetation has already received N deposition that exceeds the critical load in 2000 (Dentener et al., 2006). The most affected regions are Eastern Europe (80%), South Asia (60%) and East Asia (40-50%). This percentage will be 40% for the world's protected areas in 2030 (Bleeker et al., 2011). Elevated S and N deposition are also associated with a host of environmental issues such as acidification and eutrophication of the terrestrial system (Bouwman et al., 2002), loss of ecosystem biodiversity (Bobbink et al., 2010), harming the heterotrophic respiration and disturbing the soil decomposition process (Janssens et al., 2010), although some studies found increasing N deposition could benefit the carbon uptake by land processes (Reay et al., 2008; Holland et al., 1997). Similar to the terrestrial system, over-richness of S and N

deposition is also a threat to the aquatic system by acidification (Doney et al., 2007) and eutrophication of the ocean (Bergstrom and Jansson, 2006; Jickells, 2006; Jickells et al., 2017).

In order to understand S and N deposition, a number of global scale studies have been conducted in the last decade. Dentener et al. (2006) investigated the current (2000) and future (2030) S and N deposition with multi-model ensemble results of ACCENT IPCC-AR4 experiment (PhotoComp). Model evaluation showed that 60-70% of modelled wet deposition is within ±50% of measurements in Europe and North America. NH_x deposition was overestimated in South Asia and NO_y deposition was underestimated in East Asia. 11% of the world's nature vegetation received N deposition that exceed the critical load in 2000, and this percentage would increase to 17% under current air quality legislation and 25% under IPCC SRES A2 scenario in 2030. Sanderson et al. (2008) used the ensemble results of the 1st phase of the Task Force Hemispheric Transport of Air Pollution (HTAP I) to estimate the long-range transport of oxidized nitrogen between Europe, North America, South Asia and East Asia. Results showed that 8-15% of NO_x from source regions could be transported beyond the distance of 1000 km, which indicated the impact of inter-continental transport of air pollutants on deposition. Lamarque et al. (2013) calculated the S and N deposition in 2000 using a multi-model ensemble of the Atmospheric Chemistry and Climate Model Intercomparison Project (ACCMIP). Model performance on NO_3^- wet deposition was comparable with PhotoComp and HTAP I, but NH_4^+ wet deposition was not well simulated. Simulations with the projected emissions in 2100 under four Representative Concentration Pathways (RCP) indicated that N deposition is likely to substantially increase in Latin America, Africa and parts of Asia (especially South Asia) in the future. Vet et al. (2014) conducted a comprehensive evaluation on the model performance of HTAP I. The results underestimated the wet deposition at observation sites with high observed N deposition in North America, Southern and Northern Europe and East Asia. Dry deposition in the Unites States was found to deviate with inferential dry deposition data. Kanakidou et al. (2016) used the ACCMIP simulation results under historical, RCP6.0 and RCP 8.5 emission scenarios to estimate the changes in N deposition driven by human activity in the past (1850), present (2005) and future (2050). Their results showed that organic nitrogen (ON) from primary emission and secondary organic aerosol (SOA) account for 20-30% of total N deposition. The impact of human activity on N deposition has increased from 15% in the past to 60% in present years. This impact was likely to persist in the future. Bian et al. (2017) examined the possible factors

causing the inter-model diversity in simulating NO_3^- and NH_4^+ deposition by comparing the results of 9 models participating in the 3rd phase of Aerosol Comparisons between Observations and Models (AeroCom III). The results showed that models have large differences in calculating the pH adjustment for the effective Henry's law constant, which could largely influence the simulation of NH_x wet deposition.

These studies give a clear view to S and N deposition in the early 2000s. However, large changes are seen in the global N emissions in the last decade (van der A et al., 2008), including a large increase in China (Zhang et al., 2009b; van der A et al., 2006; Richter et al., 2005; Kurokawa et al., 2013; Zhang et al., 2007; Li et al., 2017), and general decreases in both Europe (Tørseth et al., 2012) and Eastern United States (Kim et al., 2006). In addition, ground observations and satellite measurements show large increases in the dry deposition in the western United States, Eastern Europe and East China, together with decreases in Eastern United States, Western Europe and Japan (Jia et al., 2016). Thus, a follow-up study is needed to update our knowledge about the S and N deposition with emission changes in the 21st century.

In this study, we use the multi-model mean (MMM) of 11 global models from the 2nd phase of HTAP (HTAP II) project to calculate the S and N deposition in 2010. Section 2 gives a short description of the HTAP II project and introduces the method to develop MMM and metrics for model evaluation. Section 3.1 evaluates MMM performance on wet deposition with observations from networks in North America, Europe and East Asia. The modelled dry deposition is compared with the inferential data in North America (see detail in Section 3.1). We also compare the model performance of this study with previous studies in 2001 of PhotoComp (Dentener et al., 2006), HTAP I (Vet et al., 2014), and ACCMIP (Lamarque et al., 2013). Section 3.2 and Section 3.3 estimate the S and N deposition on continental, coastal and ocean regions in 2010. By comparing our results with deposition in 2001 of HTAP I, we investigate the changes of deposition in the past 10 years. We conclude with the findings in Section 4.

2 Methodology

2.1 Model description and Experiment setup

The HTAP was developed in 2005 aiming at understanding the long-range transport of air pollution and its impact on regional air quality. HTAP I has involved more than 20 global models with base simulation year of 2001. A comprehensive assessment has been published to

summarize the findings in HTAP I with respect to the long-range transport of (1) ozone and particulate matter (2) mercury and (3) persistent organic pollutants (HTAP, 2010). The HTAP II was launched in 2012 with base year of 2010. A prescribed emission inventory called HTAPv2.2 is used by models from different groups to facilitate a fair evaluation of the models' ability and uncertainty (Galmarini et al., 2017). It is a harmonized emission inventory formed by the best estimation of emissions from different organizations, including Environmental Protection Agency (EPA) of United States, the EPA and Environment Canada, the European Monitoring and Evaluation Programme (EMEP) and the Netherlands Organisation for Applied Scientific Research (TNO), the Model Inter-Comparison Study for Asia (MICS-Asia III) and the Emission Database for Global Atmospheric Research (EDGARv4.3). The development of the emission inventory is described in Janssens-Maenhout et al. (2015). Following are some highlight findings in HTAP II. Stjern et al. (2016) estimated the impact of domestic and foreign emission change of BC, OC and SO_4 on regional radiative forcing. Huang et al. (2017) studied the impact of intercontinental outflow from East Asia to North America on O_3 pollution by simulating the regional-scale Sulfur Transport and dEposition Model (STEM) with boundary conditions provided by 3 global transport models. Jonson et al. (2018) conducted a source apportionment for O_3 pollution in Europe and calculated the contributions of emission from global wide. Tan et al. (2018) investigated the intercontinental export of sulfur and nitrogen emission and its impact on local deposition.

Among the 20 models participating in the HTAP II project (configurations described in Stjern et al. (2016)), 11 models (i.e. CAM-Chem, CHASER_re1, CHASER_t106, EMEP_rv48, GEMMACH, GEOS5, GEOSCHEMAJOINT, OsloCTM3v.2, GOCARTv5, SPRINTARS and C-IFS_v2) submitted the model outputs of S and N deposition. To develop the MMM, all models are interpolated to a uniform 0.1° × 0.1° horizontal resolution (the same resolution as the emission inventory) by linear interpolation. Then the MMM of the emission/deposition quantities of each of S and N is calculated by averaging (arithmetic mean) all available model outputs. More details are demonstrated in Section 2.2. The base year of simulation is 2010, with additional six-month run as model spin-up. The administrative boundaries of 17 regions are shown in Fig. S1. Details about the experiment setup can be found in Galmarini et al. (2017).

2.2 Method for calculating the MMM

To make the discussion clear, we define the terms as follows: The continental regions refer to all land regions including the Antarctic. The coastal regions are defined in Fig. S1. In section 3.2 and 3.3, the S deposition contains gas phase SO_2 deposition and aerosol SO_4^{2-} deposition. The N deposition includes oxidized nitrogen (NO_y) deposition and reduced nitrogen (NH_x) deposition. NO_y deposition is composed of all oxidized nitrogen species except N_2O. Based on the model outputs, NO_y deposition mainly includes NO_2, HNO_3, aerosol NO_3^-, peroxyacyl nitrate (PAN) and other organic nitrates than PAN (Orgn). NH_x deposition consists of gas phase NH_3 deposition and aerosol NH_4^+ deposition. Before constructing the MMM, we check the quality of model outputs using two criteria. First, we check the mass balance of each of the models by comparing the global deposition of each with its emission. Models are excluded if their deposition values fall outside the range of ±20% of their emission values. The second criterion is to check if the result of a model is away from the mean value of all models. We adopt the upper and lower limits as median of models ± 1.5 × interquartile by Vet et al. (2014) and check the values separately for all species of deposition and emission. The models used to develop the MMM and their values are summarized in Table S1-S3. After the quality check, we calculate the mean value of each species using equation (1) with all available model outputs. Then, we combine all of the related species into total deposition/emission by equation (2).

$$S_{MMM}(j) = \frac{1}{n}\sum_{i=1}^{n} S_i(j) \quad (1)$$

$$S_{MMM}(NO_y, NH_x \text{ or } S) = \sum_{j=1}^{s} S_{MMM}(j) \quad (2)$$

For both equations (1) and (2), i is the individual model and j is the species of deposition/emission from model outputs. $S_i(j)$ is the species j from model i and $S_{MMM}(j)$ is the MMM of species j.

2.3 Model evaluation metrics

To compare the model performance with previous projects consistently, we adopt the following metrics in Lamarque et al., (2013): Linear fit slope, mean bias, mean observation, mean model, correlation coefficient (R) and fraction (of model results) within ± 50% (of observations).

In addition, we use 4 statistical metrics following Eq. (3)-(6).

$$\text{NMB (normalized mean bias)} = \frac{\sum_{i=1}^{n}(M_i - O_i)}{\sum_{i=1}^{n} O_i} \times 100 \quad (3)$$

$$\text{NME (normalized mean error)} = \frac{\sum_{i=1}^{n} |M_i - O_i|}{\sum_{i=1}^{n} O_i} \times 100 \quad (4)$$

$$\text{MFB (mean fractional bias)} = \frac{1}{n} \sum_{i=1}^{n} \frac{M_i - O_i}{(M_i + O_i)/2} \times 100 \quad (5)$$

$$\text{MFE (mean fractional gross error)} = \frac{1}{n} \sum_{i=1}^{n} \frac{|M_i - O_i|}{(M_i + O_i)/2} \times 100 \quad (6)$$

For equations (3)-(6), M_i is the model result, O_i is the observation and n is the sample size. NMB, NME, MFB and MFE normalize the model mean bias to avoid data inflation in case of large data range. NMB and NME normalize the mean bias by the observation data and thus may tend toward model overestimation. MFB and MFE normalize the mean bias by the average of observations and model results, considering both model overestimation and underestimation, and thus are less biased. In Section 3.1, we use MFB and MFE as the main metrics to evaluate the model performance.

3 Results

3.1 Evaluation of model performance

3.1.1 Wet deposition

We evaluate the MMM results of SO_4^{2-}, NO_3^- and NH_4^+ wet deposition with site observations in United States, Europe and East Asia. The MMM result is annual deposition in 2010 and the observation data is 3-year annual average deposition during 2009-2011. The observation data in United States comes from the National Atmospheric Deposition Program (NADP) (http://nadp.sws.uiuc.edu/). The quality and completeness of the observations are checked according to the 4 criteria established by the NADP technical committee (http://nadp.sws.uiuc.edu/documentation/notes-depo.html). As a result, we use the data from 136 stations of the 267 available stations. The observations in Europe are derived from the European Monitoring and Evaluation Programme (EMEP) CCC reports (http://www.nilu.no/projects/ccc/reports.html). After checking the data quality and completeness, we use the data from 82 stations of the 102 available stations. The observations in Asia are from the Acid Deposition Monitoring Network in East Asia (EANET) (http://www.eanet.asia/). Data from 43 stations of the 52 available stations are used for evaluation.

Fig. 1 shows the scatter plots of the MMM SO_4^{2-}, NO_3^- and NH_4^+ wet deposition with observations at the NADP, EMEP and EANET stations. Performances of individual models can

be found in Fig. S2-S4 in the supplementary material. The SO_4^{2-} wet deposition comprises gas phase SO_2 and aerosol SO_4^{2-} wet deposition. The NO_3^- wet deposition includes gas phase HNO_3 and aerosol NO_3^- wet deposition. The NH_4^+ wet deposition contains gas phase NH_3 and aerosol NH_4^+ wet deposition. Performance of individual models can be found in Figs. S2-S4 in the supplementary material. Fig. 2 displays the spatial distributions of MMM SO_4^{2-}, NO_3^- and NH_4^+ wet deposition (contours) with observations (filled circles). In terms of SO_4^{2-} wet deposition, the MMM results are consistent with observations at the NADP stations with a close to 1 slope (0.9) and a high R value (0.8) (Fig.1 (a)). The MFB and MFE are 9% and 32%, indicating slight overestimation. According to Fig. 2(a), the observed SO_4^{2-} wet deposition is highest in northeastern United States, and this spatial distribution is well captured by MMM. The EMEP stations are well simulated with low MFB (-7%) and MFE (25%) (Fig. 1(b)). The MMM predictions are within ±50% of observations at 87% of the stations. According to Fig. 2(b), 1 station in Poland and 1 station in Norway, with observed SO_4^{2-} wet deposition of 1000 and 500 mg (S) m^{-2} yr^{-1} respectively, are underestimated by 50%. We evaluate the model performances on simulating precipitation (Fig. S5 and Fig. S6). For the Norway site, the observed precipitation is 1566 mm yr^{-1} and the mmm underestimated the precipitation by 49%, which fits well for the 50% underestimation of SO_4^{2-} wet deposition at this site. For the Polish site, the observed precipitation is 1137 mm yr^{-1} and the mmm underestimated the precipitation by 21%. The underestimation in precipitation could partly explain the negative model bias in simulating SO_4^{2-} wet deposition. Another possible reason is the high topography of the sites. The Polish site is 1603 meters above sea, which is one of the highest sites among the European sites. Similar to the Polish site, one site in Spain, which is 1360 meters height, is underestimated by 142 mg (S) m^{-2} yr^{-1} (59%) for SO_4^{2-} wet deposition, while its precipitation is well simulated with a slight positive model bias of 5%. At the EANET stations, very high SO_4^{2-} concentrations were measured at some stations, probably correlated with dust emission (Dentener et al., 2006). Therefore, we ignore the measurements coincident with measured calcium (Ca^{2+}) deposition larger than 20 mole m^{-2} yr^{-1}. The evaluation (Fig. 1(c)) shows that the SO_4^{2-} wet deposition is generally underestimated at the EANET stations by 23% (MFB) and 44% (MFE). The stations in Korea and Vietnam are generally underestimated by more than 200 mg (S) m^{-2} yr^{-1} (Fig. 2(c)). On the other hand, the SO_4^{2-} wet deposition is generally well simulated in Indonesia, Philippines, Thailand and Japan. Overall, 76% of the stations of all networks predicted quantities within

±50% of observations. The EANET stations have the highest model bias among the 3 networks. It should be noted that for the 3 excluded stations (located in China) with high Ca^{2+} deposition, the SO_4^{2-} wet deposition is largely underestimated by more than 1000 mg (S) m^{-2} yr^{-1} (not shown in figures). If we include these stations in the model evaluation, the mean bias for East Asia changes from -160 mg (S) m^{-2} yr^{-1} to -300 mg (S) m^{-2} yr^{-1}. We also realize that the observation stations in China are mainly located along the eastern and southern coast, while the highest modelled deposition is found in the inland areas. Therefore, it is hard to conduct a comprehensive evaluation over this region due to unavailable measured data in the inland areas.

For NO_3^- wet deposition, the MMM results agree well with observations at the NADP stations, as shown by the linear regression line in Fig. 1(d) with slope of 1.2 and R value of 0.9. However, the amount of deposition is overestimated by 33% (MFB) and 36% (MFE). According to Fig. 2(d), there is a general tendency of overestimation throughout the stations in United States, especially the stations located in Midwest and Southeast. At the EMEP stations, the NO_3^- wet deposition is well simulated with low MFB of -5% and MFE of 24% (Fig. 1(e)). The modelled deposition is within ±50% of observed deposition at more than 90% of the stations. The MMM results are close to the observations at stations with deposition lower than 400 mg (N) m^{-2} yr^{-1}, but generally underestimate the deposition at stations with higher observations. According to Fig. 2(e), wet deposition at 3 stations in Poland, Norway and Spain were underestimated by 430 (59%), 420 (63%) and 290 (67%) mg N m^{-2} yr^{-1}, respectively. Besides, the stations in Germany generally under-predict these values by 100-200 mg (N) m^{-2} yr^{-1}. The NO_3^- wet deposition at the EANET stations is well simulated with MFB (-3%) and MFE (43%) (Fig. 1(f)). The model estimations are within ±50% of observations for 77% of the stations. According to Fig. 2(f), 1 station in Central China is overestimated by 400 (130%) mg (N) m^{-2} yr^{-1}. On the contrary, 3 stations in Thailand, Vietnam and Malaysia are underestimated by 570 (78%), 350 (66%) and 200 (64%) mg (N) m^{-2} yr^{-1}. Overall, 83% of the MMM results are within ±50% of observations at stations of all networks. The NADP stations have the highest MFB due to a generally positive bias in the eastern United States. The EANET stations have the highest MFE value, mainly due to the underestimation in Southeast Asia.

The modelled NH_4^+ wet deposition agrees well with observations at the NADP stations with MFB of 7% and MFE of 25% (Fig. 1(g)). 88% of modelled deposition is within ±50% of observations as shown by the R value of 0.9. The MMM has well captured the high deposition in

the United States Midwest, but slightly underestimates the deposition in the Southeast (Fig. 2(g)). At the EMEP stations, the NH_4^+ wet deposition is well simulated with MFB of -1% and MFE of 36% (Fig. 1(h)). The MMM results are close to the observations at most stations and well reproduce the high deposition in Germany and Italy (Fig. 2(h)). Some stations in Norway and Poland are slightly underestimated by 100-200 mg (N) m^{-2} yr^{-1}. These stations all report observations of higher deposition than 500 mg (N) m^{-2} yr^{-1}. The NH_4^+ wet deposition is underestimated at the EANET stations by 10% (MFB) and 50% (MFE) (Fig. 1(i)). The MMM has well captured the high deposition in Eastern China and Indonesia, but generally underestimates the NH_4^+ wet deposition at the Russian stations (Fig. 2(i)). In addition, the observed deposition at the 3 Korean stations is relatively high (~500-600 mg (N) m^{-2} yr^{-1}), but the MMM fails to reproduce any of them. There could be a missing emission source in that region. Overall, 81% of the MMM predictions are within ±50% of observations at stations of all networks. The NH_4^+ wet deposition is somewhat underestimated in all 3 regions, especially in East Asia.

Table 1 compares the model performance of this study (HTAP II) with previous projects of PhotoComp (Dentener et al., 2006), HTAP I (Vet et al., 2014) and ACCMIP (Lamarque et al., 2013). It should be noted that the emission inputs, simulation periods and participating groups of this study (year 2010) are different from those of the previous projects (year 2001). Although the observations are from the same networks, the previous projects used 3-year averaged observations of 2000-2002 and this study used those of 2009-2011. Due to these differences, the model performances may not be totally comparable. In terms of SO_4^{2-} wet deposition, the model performance is similar to that for previous projects in North America, with 4-6% higher percentage of stations within ±50% of observations. Large improvement is found in Europe. The absolute mean bias decreases from 50-130 mg (S) m^{-2} yr^{-1} to 30 mg (S) m^{-2} yr^{-1}. There is 10% increase in the fraction of stations within ±50% of observations. At the East Asian stations, the absolute mean bias decreases slightly from 180~290 mg (S) m^{-2} yr^{-1} to 160 mg (S) m^{-2} yr^{-1}. But the R value and fraction within ±50% have somewhat declined. For NO_3^- wet deposition, HTAP II performs similar to the ensembles used in previous projects in North America, but slightly better in Europe with lower mean bias and 5% increase in the fraction within ±50% of observations. The model mean bias at the Asian stations has decreased significantly from ~50 mg (N) m^{-2} yr^{-1} to ~1 mg (N) m^{-2} yr^{-1}. However, the biases for individual models are large (Fig.

S3). Large negative model bias is found in Southeast Asia and improvements are needed in the future. In terms of NH_4^+ wet deposition, HTAP II shows similar R values to those of ensembles used for the previous projects at the NADP stations, with slightly lower model bias. However, HTAP II shows considerable improvement in Europe. The slope of the regression line increases from 0.3-0.4 to 0.6 and the mean bias decreases from as large as -95 mg (N) m^{-2} yr^{-1} to -4 mg (N) m^{-2} yr^{-1}. For Asia, the slope, mean bias and R values for HTAP II are all within the ranges of the previous projects, while the absolute mean bias decreases form 70~140 mg (N) m^{-2} yr^{-1} to 30 mg (N) m^{-2} yr^{-1}.

3.1.2 Dry deposition

The number of dry deposition measurements is limited due to difficulty in measuring the dry deposition directly by instruments. This study evaluates the dry deposition in United States using information from the Clean Air Status and Trends Network (CASTNET). Instead of direct measurements, the data are produced by an "inferential" method, using calculations of the measured concentration of species and modelled dry deposition velocities. We use the 3-year average data of 2009-2011 from CASTNET and adopt the same selection criteria as we did for the wet deposition measurements. Data from 81 stations out of 85 available stations is used for comparison. Fig. 3 shows the scatter plots of the MMM SO_2, SO_4^{2-}, NO_3^-, HNO_3 and NH_4^+ dry deposition with inferential data at the CASTNET stations. Performances of individual models can be found in Fig. S7-S11 in the supplementary material. The modelled SO_2 dry deposition is 240 (170%) mg (S) m^{-2} yr^{-1} higher than the inferential data and only 5% of the stations is within ±50% of the inferential values. There are smaller discrepancies for values of SO_4^{2-} dry deposition (14 mg (S) m^{-2} yr^{-1} and 60%) between model and inferential results. Modelled NO_3^-, HNO_3 and NH_4^+ dry deposition is generally 50-100% higher than the inferential data and the fraction within ±50% is about 15%. Fig. 4 shows the spatial distributions of MMM dry deposition (contours) with the inferential data (filled circles). The MMM results are consistent with the inferential data in the western United States, where the dry deposition is generally low. And both datasets predict high NO_3^- dry deposition in western California. Large disagreements are found in the eastern United States. In the Midwest (mainly Indiana and Ohio states), although both results estimate higher N (NO_3^-, HNO_3 and NH_4^+) dry deposition in this region than the others, the prediction of MMM is 20-30 mg (N) m^{-2} yr^{-1} higher than the inferential data at every station. In addition, the

MMM estimates much higher deposition in southern and northeastern United States than in the western United States, but this gradient is much weaker in the inferential data.

Table 2 compares the model performance of this study (HTAP II) with that of the models used in the previous projects of HTAP I (Vet et al., 2014) and ACCMIP (Sun et al., 2017). HTAP I used the 2001 simulation results and compared them with 3-year average (2000-2002) CASTNET data. ACCMIP used 10-yr averages of both MMM and CASTNET data from 2000 to 2009. The N dry deposition values for all projects contain NO_3^-, NH_4^+ and HNO_3 and the S dry deposition includes SO_2 and SO_4^{2-}. Both HTAP I and HTAP II overestimated the S and N dry deposition, but HTAP II has ~100 mg(S) m^{-2} yr^{-1} and ~80 mg(N) m^{-2} yr^{-1} lower mean bias than HTAP I. The comparison with ACCMIP results may not be solid since there are large differences in simulation periods. Generally, the HTAP II performance is similar to ACCMIP for NH_4^+, SO_2 and SO_4^{2-} dry deposition simulation, but has larger mean bias for HNO_3 dry deposition prediction.

Since the CASTNET dry deposition is not actually measured but instead a calculation of measured concentration of species and modelled dry deposition velocities, it is necessary to investigate which factor of these two contributes to the model bias. We compare the modelled air pollutant concentrations with CASENET measurements as shown in Table S4-S8. The MMM overestimates the SO_2, SO_4^{2-}, HNO_3, NO_3^- and NH_4^+ concentrations by 394%, 40%, 217%, 135% and 173%, respectively. It should be noted that the CASTNET sites are generally located in rural regions that are away from emission sources (Sickles and Shadwick, 2008), thus the measured concentrations of air pollutants are relatively low compared with those of urban sites. While the resolutions of the HTAP II models range from 0.5° to 3°, and are not fine enough to reproduce the characteristic of some rural sites. The models with finer resolutions except CHASER_t106 model (i.e. EMEP_rv48 (0.5° × 0.5°) and SPRINTARS (1.1° × 1.1°)) generally perform better than the others, while models with coarse resolutions (i.e. CHASER_re1 (2.8° × 2.8°) and OsloCTM3.v2 (2.8° × 2.8°)) are generally not performing well for all species. This could explain the overestimation of air pollutant concentrations at the CASTNET sites.

In order to check the differences of modelled dry deposition velocity between CASNET and HTAP II models, we adopt the general approach for calculating dry deposition velocity from Wesely, (1989).

$$V_d = -F_c / C_a \qquad (7)$$

Where V_d is the deposition velocity, F_c is the dry deposition flux and C_a is the concentration of species. The negative mark indicates the direction of the dry deposition velocity. This scheme has been widely adopted in global models (Wesely and Hicks, 2000) with modifications. We compare the calculated dry deposition velocity of models and CASTNET (Table S9-S13). The mean bias of dry deposition velocities for MMM are -8%, 0.3%, 7%, 19% and 2% for SO_2, SO_4^{2-}, HNO_3, NO_3^- and NH_4^+, respectively, which are much lower than those of air pollutants. The model bias for dry deposition at the CASTNET sites mainly comes from the model over prediction of air pollutant concentration.

In addition, the CASENET estimation of dry deposition has been reported with uncertainties. Zhang et al. (2009a) estimated a 10-20% uncertainty in the measurement of mixing ratio of species, 20% in the calculated velocity and ~20% when lacking of hourly concentration for species with strong diurnal variation. Schwede et al. (2011) compared CASTNET dry deposition estimates with those of the Canadian Air and Precipitation Monitoring Network (CAPMoN). The CASTNET data is 54% lower for SO_2 dry deposition and 47% lower for HNO_3 dry deposition than CAPMoN, mainly due to using different models to calculate the dry velocity.

3.2 Total S deposition

Table 3 lists the calculated amount of S emission and deposition on continents, coastal regions and oceans. Fig. 5 presents the distribution of S emission and deposition from MMM results. The distributions of components of S deposition are shown in Fig. S12 in the supplementary material. The global S deposition is 84 Tg(S) in 2010, with 49% deposits on non-coastal continents, 32% deposits on non-coastal ocean and 19% deposits on coastal area. For continental non-coastal regions, East Asia receives the largest amount of S deposition (17%). The highest S deposition is found in Eastern China (2000 mg(S) m^{-2} yr^{-1}) (Fig. 5(b)). Other regions with largely extended areas of high S deposition are the Indian peninsula (800-1200 mg(S) m^{-2} yr^{-1}), Malaysia and Indonesia (~1200 mg(S) m^{-2} yr^{-1}), United States Midwest (800-2000 mg(S) m^{-2} yr^{-1}), Mexico and Central America (400-800 mg(S) m^{-2} yr^{-1}), Peru and Chile (400-600 mg(S) m^{-2} yr^{-1}), Eastern Europe (~800 mg(S) m^{-2} yr^{-1}) and the northeastern Middle East (500-1200 mg(S) m^{-2} yr^{-1}). The distribution of high deposition regions agrees very well with high S emission regions (Fig. 5(a)). For coastal regions, East Asia and Southeast Asia receive the most S deposition (3% and 3% respectively). The east coast of East Asia and North America and

all of the coast of India have relatively high deposition (400-800 mg(S) m^{-2} yr^{-1}), followed by the west coast of Mexico (~400 mg(S) m^{-2} yr^{-1}). This study estimates 43 Tg(S) of S deposition on the ocean and coastal regions in 2010, and accounts for 51% of global S deposition. The ratio is similar to the 51% estimated by Dentener et al. (2006) and 46% estimated by Vet et al. (2014) in 2001.

We calculate the ratio of S deposition to S emission (Fig. 5(c)). Because it is not clear how dimethyl sulphide (DMS) emission will transfer to S deposition, this ratio does not represent the transformation of S emission to deposition. For continental non-coastal regions, the average ratio is 85% (86% if taking consideration of coastal regions). In high emission regions, this ratio can be viewed as the "scavenging" effect of S pollution by deposition. In major source regions of S emission (i.e. North China Plain, Midwest of United States and India), the ratios are only slightly higher than 50%, while in low S emission regions (<10 mg(S) m^{-2} yr^{-1}), the ratios could exceed 400 % (areas with white color in Fig. 5(c)). This result indicates that the deposition in these regions is largely affected by long-range transport of pollution from other regions. The impact of intercontinental transport of air pollutants on deposition can be quantified by the emission perturbation experiments in HATP II. Results from those experiments will be discussed in another paper (Tan et al., 2018).

We compare the S emission and deposition in 2010 from HTAP II with that in 2001 from HTAP I (Vet et al., 2014) (Table 3). We re-calculate the HTAP I results according to the regions defined in HTAP II (Fig. S1), so the HTAP I results may look different from those in Table 2 of Vet et al. (2014). Because different models were used for each of the two ensembles compared, associated uncertainty is expected. In addition, emissions in HTAP I were not prescribed, so each modelling group used its own best estimation of emissions (Sanderson et al., 2008). Conversely, all models in HTAP II, used the same anthropogenic emission values (although there were still differences in natural emission). Globally, the S emission decreases by 5 Tg(S) from 2001 to 2010, with 8 Tg(S) (13%) decrease in continental non-coastal regions, 6 Tg(S) (32%) increase in non-coastal ocean regions and 3 Tg(S) (15%) decrease in coastal regions. For continental non-coastal regions, there are big drops in S emissions from Europe (6 Tg(S) and 61%), North America (3 Tg(S) and 34%) and Russia (2 Tg(S) and 44%). On the other hand, South Asia and Middle East have 2 Tg(S) (56%) and 1 Tg(S) (69%) increase in S emissions. East Asia, one of the main contributors to S emission seems to show little change between 2001 and 2010.

However, it has experienced large changes during these 10 years, with stable annual increases from 2000 to 2005 due to increased energy consumption and decreases after 2006 owing to the successful implementation of the SO_2 control policies in China's 11th Five-Year-Plan (FYP) (Lu et al., 2010). For coastal regions, Europe has experienced a 2 Tg(S) (54%) decrease and East Asia has experienced a 1 Tg(S) (43%) decrease in S emission. Other regions have relatively small (0-0.6 Tg(S)) changes. The global S deposition decreases by 2 Tg(S), with 5 Tg(S) (11%) decrease in continental non-coastal regions, 4 Tg(S) (16%) increase in non-coastal ocean regions and 1 Tg(S) (5%) decrease in coastal regions. The regions with the largest change in deposition coincide with those having big changes in emission. For instance, Europe experiences 5 Tg(S) decrease in S deposition with 8 Tg(S) decrease in emission, and South Asia receives 2 Tg(S) more S deposition with 2 Tg(S) increase in emission. Fig. S13(b) compares the S deposition in HTAP II with that in HTAP I. Declined S deposition is found in large areas of the eastern United States and Europe (400-1,500 mg(S) m^{-2} yr^{-1}). Regions with increased S deposition are India and Indonesia (100-800 mg(S) m^{-2} yr^{-1}). In China, there is a mixture of both increases and decreases in S deposition over different areas. The changes in S depositions agree well with changes in S emissions (Fig. S13(a)). During China's 11th FYP, one of the main technologies to control the SO_2 emission was to install the Flue Gas Desulfurization (FGD) on power plants (Cao et al., 2009). The effectiveness of this technology in removing SO_2 emission varies considerably regionally, as a result of several factors such as the coverage of FGD technology on power plants, local reduction targets and stringency of policy implementation by local governments. On the other hand, new sources of SO_2 emission, such as newly built power plants, are found responsible for the increased S emissions and deposition over some areas in China (Tan et al., 2017).

3.3 Total N deposition

3.3.1 NO_y deposition

Table 4 summarizes the NO_y emission and deposition in each region and Fig. 6 presents the distribution from MMM results. Distributions of components of NO_y deposition are shown in Fig. S14 in the supplementary material. The global NO_y deposition is 59 Tg(N) in 2010, with 62% of deposits on non-coastal continents, 22% of deposits on non-coastal ocean and 16% of deposits on coastal areas. For continental non-coastal regions, East Asia receives the largest NO_y

deposition (14%). The highest NO_y deposition is found in northeastern China (2000 mg(N) m^{-2} yr^{-1}), followed by the Indian peninsula (800-1200 mg(N) m^{-2} yr^{-1}), Malaysia and Indonesia (500-800 mg(N) m^{-2} yr^{-1}), Germany, Switzerland and Poland (500-600 mg(N) m^{-2} yr^{-1}), northern Sub-Saharan Africa (300-500 mg(N) m^{-2} yr^{-1}), northeastern Middle East (400-500 mg(N) m^{-2} yr^{-1}), United States Midwest (500-600 mg(N) m^{-2} yr^{-1}) and Brazil (300-600 mg(N) m^{-2} yr^{-1}).

For coastal regions, the east coast of East Asia also receives the largest amount of NO_y deposition (600 mg(N) m^{-2} yr^{-1} and 4%). Relatively high deposition is found on the east coast of North America (150-400 mg(N) m^{-2} yr^{-1}), all of the coast of India (300-500 mg(N) m^{-2} yr^{-1}), the west coast of Europe and all of the coast of Southeast Asia (150-200 mg(N) m^{-2} yr^{-1}). This study estimates 23 Tg(N) of NO_y deposition on the ocean in 2010 (include ocean non-coastal and coastal), similar to Dentener et al. (2006)'s estimation of 23 Tg(N), Duce et al. (2008)'s estimation of 14-32 Tg(N) and Vet et al. (2014)'s estimation of 20 Tg(N). About 38% of global NO_y deposits on the ocean, lower than 43% in PhotoComp (Dentener et al., 2006) and 42% in HTAP I (Vet et al., 2014), but higher than 30% estimated by Lamarque et al. (2005). It should be noted that these values partly depend on the land-ocean mask, which may differ among different studies. For non-coastal ocean regions, the NO_y deposition is 13 Tg(N), accounts for 22% of the global deposition. While the emission from oceans is only 2 Tg(N), about 4% of global emission. The difference of 11 Tg(N) indicates NO_y transport from continents to the open ocean. Antarctic have near zero NO_x emission, but receive 0.1 Tg(N) NO_y deposition. Deposition has been a non-negligible pathway that human pollution is contaminating the nearly untouched areas.

We calculate the ratio of NO_y deposition to NO_x emission (Fig. 6(c)). In continental non-coastal regions, the average ratio is 74% (81% if taking consideration of coastal regions). In high NO_x emission regions (i.e. North America, East Asia and South Asia), an average 60-80% of the NO_y is removed by deposition, with large regional variation. For low emission regions (i.e. North Africa and Central Asia), the ratio can reach higher than 90%. Also in coastal regions and open ocean, the ratio is generally over 200%. Instead of the local emission, the transport of air pollutants from elsewhere is the major source of deposition.

3.3.2 NH_x Deposition

The global NH_x deposition is 54 Tg(N) in 2010, with 69% of deposits on continental non-coastal regions, 19% of deposits on ocean non-coastal regions and 13% of deposits on coastal regions

(Table 4). For continental non-coastal regions, South Asia receives 16% of global NH_x depositions, followed by East Asia (13%). The whole Indian peninsula receives higher NH_x depositions than 2,000 mg(N) m^{-2} yr^{-1} (Fig. 6(e)). Also, the Asian regions have several high deposition areas: the North China Plain and Indonesia (1,200-2,000 mg(N) m^{-2} yr^{-1}), Japan, Thailand, Vietnam and Myanmar (500-600 mg(N) m^{-2} yr^{-1}). Other regions with high NH_x deposition are: the United States Midwest, Germany, France, Northern Italy, Southern Brazil and Ethiopia (400-800 mg(N) m^{-2} yr^{-1}). Distributions of components of NH_x deposition are shown in Fig. S15 in the supplementary material.

Coastal regions of Southeast Asia (3%), East Asia (2%) and South Asia (2%) receive the largest NH_x deposition (~200-400 mg(N) m^{-2} yr^{-1}). The east coast of North America and Mexico also have high NH_x deposition (150-200 mg(N) m^{-2} yr^{-1}). Compared to NO_y deposition, the NH_x deposition on coastal regions is relatively lower. The ocean receives 17 Tg(N) of NH_x deposition in 2010, within the range of 13-29 Tg(N) estimated by Duce et al. (2008), but lower than 23.5 Tg(N) estimated by Dentener et al. (2006) and 21.4 Tg(N) estimated by Vet et al. (2014). 31% of NH_3 emission is deposited on ocean areas, similar to 31% estimated by Dentener et al. (2006) and 30% estimated by Lamarque et al. (2005), but slightly lower than 37% in PhotoComp (Dentener et al., 2006) and 37% in HTAP I (Vet et al., 2014). The ocean emitted 12 Tg(N) of NH_3 in 2010, which means that at least 5 Tg(N) of NH_x deposition on oceans in 2010 came from continental regions. This value is considerably lower than the 13 Tg(N) of deposition-emission difference for NO_y (including the 2 Tg(N) difference on coastal regions). A possible explanation is that NH_3 has a short lifetime in the atmosphere, which makes it more likely to deposit close to where it is emitted (Shen et al., 2016), while NO_x can be oxidized to organic nitrate (Moxim et al., 1996), which facilitates the long-range transport from land to open ocean.

We calculate the ratio of NH_x deposition to NH_3 emission (Fig. 6(f)). The average ratio is 87% for continental non-coastal regions (92% if also considers the coastal regions). The ratios are generally higher than those of NO_y deposition (74% and 81%), since large a proportion of NH_x deposits near the source. The ratios are generally over 400% for coastal areas, but less than 100% on open ocean (70-90%). This is because there is less continental NH_x transported to the open ocean than to coastal regions.

3.3.3 N deposition

The global N deposition in 2010 is 113 Tg(N), with 65% of deposits on the continental non-coastal regions, 20% on non-coastal oceans and 15% on coastal regions (Table 4). East Asia (13%) and South Asia (11%) receive the largest amount of N deposition, consistent with the fact that they are also the largest N emission sources (16% and 13% respectively). The deposition reaches 3000 mg(N) m^{-2} yr^{-1} over Eastern China (especially North China Plain) and 2000 mg(N) m^{-2} yr^{-1} over India and Southeast Asia (Thailand, Vietnam and Malaysia). Other regions of high N deposition are the United States, northeast Western Europe (800-1200 mg(N) m^{-2} yr^{-1}), Mexico, Central America, Brazil, northern Sub-Saharan Africa and the northeastern Middle East (500-600 mg(N) m^{-2} yr^{-1}). For coastal regions, the east coast of the United States, all coasts of India and the east coast of East Asia are identified with relatively high deposition (>600 mg(N) m^{-2} yr^{-1}).

Table 5 compares the N emission and deposition in HTAP II with HTAP I. The global N emission increases from 105 Tg(N) to 115 Tg(N), with a 12 Tg(N) (15%) increase in continental non-coastal regions and a 2 Tg(N) (14%) decrease in coastal regions. The change on the ocean is small due to increased NO_y deposition but decreased NH_x deposition. For continental non-coastal regions, increases in N emission are found in South Asia (5 Tg(N), 56%), East Asia (4 Tg(N), 26%) and Southeast Asia (2 Tg(N), 58%), while the emission in Europe decreases by 1 Tg(N) (12%). The emission changes in coastal regions are relatively small. The global N deposition increases by 7 Tg(N), with a 9 Tg(N) (14%) increase in continental non-coastal regions and a 2 Tg(N) decrease in ocean regions. Asian regions also have experienced the largest increases in deposition, and the amounts are identical with corresponding emission changes. Fig. S16 (b) compares the distribution of N deposition in HTAP II with HTAP I. Elevated N deposition is found in India, Indonesia and North Chain Plain (1,500 mg(N) m^{-2} yr^{-1}). Regions with small increases are Japan, the northern Middle East, northwestern Brazil and Mexico (~200 mg(N) m^{-2} yr^{-1}). On the other hand, the N deposition in the eastern United States and Europe have decreased by 200-400 mg(N) m^{-2} yr^{-1}.

The global N dry and wet deposition is 40 Tg(N) yr^{-1} and 73 Tg(N) yr^{-1} in 2010, respectively. We calculate the ratio of dry deposition as $\frac{dry\ deposition}{dry\ deposition + wet\ deposition} \times 100\%$. For continental non-coastal regions, about 44% (range from 35-61%) of the N deposition comes from dry

deposition (42% if take coastal regions into consideration). If the overestimation of N dry deposition in Section 3.1.2 is considered, this ratio could be even lower. Desert areas (e.g., the Sonoran, Mojave and Chihuahuan deserts near the west coast of North America, the Sahara Desert in North Africa, the Arabian Desert in Middle East and the Great Victoria Desert in Australia) are seen with high ratios of dry deposition (80%) (Red color regions in Fig. 7(c)). This outcome is reasonable since these areas generally lack precipitation. Low fractions of dry deposition (30%) are found in Russia, Western China, Southeast Asia, Australia and Central America. Almost all coastal regions are dominated by wet deposition. A study by Jickells (2006) reported a dry deposition ratio of 21-45% for the east coast of the United States and a study by Baker et al. (2010) suggested a ratio of 15-22% for the Atlantic Ocean. Our study receives similar ratios for these coastal regions. A study by Bey et al. (2001) found an outflow of NO_y from Asia over the Western Pacific Ocean through deposition. According to this study, about 70% of this land-to-ocean export of NO_y deposition is through wet deposition (Fig.7 (a)).

The NH_x and NO_y deposition is 54 Tg(N) yr^{-1} and 59 Tg(N) yr^{-1} in 2010, respectively. The average ratio of NH_x deposition (calculated as $\frac{NH_x\ deposition}{NH_x\ deposition + NO_y\ deposition} \times 100\%$) for continental non-coastal regions is 47% (45% if coastal regions are taken into consideration). South Asia (71%) and Southeast Asia (63%) are dominated by NH_x deposition, owing to high local NH_3 emission, while the Middle East (25%) and North Africa (34%) are dominated by NO_y deposition. Fig. 7(f) shows the global distribution of the ratio of NH_x deposition. Except the high ratio found in the Indian peninsula, Southeast Asia, Southeast Brazil, South Argentina and New Zealand (70-80%) and Eastern Asia (~60%), other continental non-coastal regions are mainly dominated by NO_y deposition. This is consistent with finding by ACCMIP (Sun et al., 2016). We compare the ratio of NH_x deposition in 2010 (HTAP II) with that in 2001 (HTAP I) (Fig. S17). Generally, we found a 10% worldwide decrease in the ratio of NHx deposition from 2001 to 2010. In particular, a 30% decrease is found in southeastern China, mainly due to the large increase in NO_x emission during the last decade. On the other hand, the ratio of NH_x deposition in California was 15-20% in 2001 and increases to 40-60% in 2010. The ratio in Alaska also increases from 30-40% to 50%. There is a generally 5-10% increase over the eastern United States. This is consistent with an observed large increase of the NH_x depositions and decrease of NO_y depositions in northeastern United States from 1990s to 2010s (Du et al., 2014;Li et al., 2016). A possible explanation is that the implementation of emission control stretegies such as

the Clean Air Act (CAA) has resulted in a large reduction in NO_x emssions, which lowered the NO_y deposition in the United States (Lloret and Valiela, 2016). This benefit is compensated by increasing NH_x deposition because no limitation is implemented on NH_3 emission (Kanakidou et al., 2016;Li et al., 2016). Some regions have small increases in the ratio of NH_x deposition, such as North Europe (Norway) (5%), Southeast Asia (10%) and Western Australia (10%).

4 Conclusions

We calculate the S and N deposition in 2010 using the multi-model mean (MMM) of an 11-model ensemble from the HTAP II project. The model performance on wet deposition is evaluated with measurement networks of NADP over North America, EMEP over Europe and EANET over East Asia. The modelled wet deposition compares favorably with the observations. About 76-83% of stations are predicted within ±50% of observations. SO_4^{2-} wet deposition is underestimated in East Asia by 20%, especially at 3 Chinese stations with high Ca^{2+} concentration. Because the locations of the Chinese stations don't cover the areas with highest deposition, it is hard to provide a comprehensive evaluation over this region. For NO_3^- wet deposition, 20% positive model bias is generally found at stations in eastern United States, while some European (Poland, Norway and Spain) and East Asian (in Southeast Asia) stations with high observed deposition are underestimated by about 60-70%. NH_4^+ wet deposition is underestimated in Europe (especially in Norway and Poland) and East Asia (especially in Russia and Korea). An inter-comparison is conducted with previous projects of PhotoComp, ACCMIP and HTAP I. HTAP II has significantly improved the estimation of both S and N deposition at European stations compared to that in previous projects. Improved estimates are also found in East Asia. Modelled dry deposition is compared with the inferential data from CASTNET in North America. The MMM results are generally higher than the inferential data by 50-170%, which is also reported in ACCMIP and HTAP I studies.

We calculate the S and N depositions on lands, costal zones and open oceans. The global S deposition is 84 Tg(S) in 2010, with 49% deposits on continental non-coastal regions, 32% deposits on non-coastal oceans and 19% deposits on coastal regions. The global N deposition is 113 Tg(N) in 2010, of which 59 Tg(N) is NO_y deposition and 64 Tg(N) is NH_x deposition. 65% of N is deposited on the continental non-coastal regions and 35% is on oceans (including 15% on coastal regions). For continental regions, high S deposition is found in Asia regions (East Asia,

South Asia and Southeast Asia), United States Midwest, Central America and Eastern Europe. For N deposition, high deposition is also identified in the above-mentioned regions plus the Sub Sahara Africa and Brazil. For coastal regions, the east coast of Asia, all coasts of India and Malaysia and east coast of Unites States are seen with relatively high S and N deposition. According to our estimation, about 4 Tg(S) of S deposition and 18 Tg(N) of N deposition are exported from land to ocean, including 0.3 Tg(S) and 4 Tg(N) in coastal regions.

We compare the HTAP II results in 2010 with HTAP I in 2001 by using the same land-ocean mask. The S deposition decreases 2 Tg(S) from 2001 to 2010, with significant decreases in Europe (5 Tg(S)), North America (3 Tg(S)) and Russia (2 Tg(S)), and increases in South Asia (2 Tg(S)) and the Middle East (1 Tg(S)). East Asia doesn't have large net changes in its S deposition due to increased S emission from 2001-2005 and a continuous reduction in S emission starting from 2006 owing to the SO_2 control policies in China's 11th FYP. The N deposition increases by 7 Tg(N). The increased N emissions from South Asia (5 Tg(N)), East Asia (4 Tg(N)) and Southeast Asia (2 Tg(N)) lead to identical amounts of elevation in deposition in corresponding regions. We also compare the ratio of NH_x deposition in total N deposition between HTAP I and HTAP II. The ratio has increased in some regions of North America, especially in California (~20%), Alaska (~10%) and the eastern United States (5-10%), which agrees well with recent observational and modelling studies in United States. A small increase in the ratio of NH_x deposition is found in North Europe (Norway) (5%), Southeast Asia (10%) and Western Austrilia (10%). On the other hand, NO_y deposition starts to dominate in East Asia (especially China) due to increased NO_x emission in recent years.

This study updates our knowledge about the global S and N deposition in 2010. We find that the global distributions of S and N depositions have changed considerably during the last 10 years, with decreases in North America and Europe and increases in Asian regions. Further studies could determine how much these changes could affect the source-receptor relationship on deposition between continents and the impact of this relationship on global agriculture and ecosystems?

Acknowledgements

We thank all participating modelling groups in HTAP II for providing the simulation data. We thank Dr. Robert Vet for providing the multi-model ensemble results of HTAP I. The National Center for Atmospheric Research is sponsored by the National Science Foundation. The CESM

project is supported by the National Science Foundation and the Office of Science (BER) of the U.S. Department of Energy. Computing resources were provided by the Climate Simulation Laboratory at NCAR's Computational and Information Systems Laboratory (CISL), sponsored by the National Science Foundation and other agencies. We acknowledge the support by NASA HAQAST (grant no. NNX16AQ19G). We also acknowledge the support by Supercomputer system of the National Institute for Environmental Studies, Japan and The Environment Research and Technology Development Fund (S-12-3) of the Ministry of the Environment, Japan, JSPS KAKENHI (grant no. 5H01728).

References

Baker, A. R., Lesworth, T., Adams, C., Jickells, T. D., and Ganzeveld, L.: Estimation of atmospheric nutrient inputs to the Atlantic Ocean from 50 degrees N to 50 degrees S based on large-scale field sampling: Fixed nitrogen and dry deposition of phosphorus, Global Biogeochem Cy, 24, 10.1029/2009gb003634, 2010.

Bergstrom, A. K., and Jansson, M.: Atmospheric nitrogen deposition has caused nitrogen enrichment and eutrophication of lakes in the northern hemisphere, Global Change Biol, 12, 635-643, 10.1111/j.1365-2486.2006.01129.x, 2006.

Bey, I., Jacob, D. J., Logan, J. A., and Yantosca, R. M.: Asian chemical outflow to the Pacific in spring: Origins, pathways, and budgets, J Geophys Res-Atmos, 106, 23097-23113, 10.1029/2001jd000806, 2001.

Bian, H. S., Chin, M., Hauglustaine, D. A., Schulz, M., Myhre, G., Bauer, S. E., Lund, M. T., Karydis, V. A., Kucsera, T. L., Pan, X. H., Pozzer, A., Skeie, R. B., Steenrod, S. D., Sudo, K., Tsigaridis, K., Tsimpidi, A. P., and Tsyro, S. G.: Investigation of global particulate nitrate from the AeroCom phase III experiment, Atmospheric Chemistry and Physics, 17, 12911-12940, 2017.

Bleeker, A., Hicks, W. K., Dentener, E., Galloway, J., and Erisman, J. W.: N deposition as a threat to the World's protected areas under the Convention on Biological Diversity, Environ Pollut, 159, 2280-2288, 2011.

Bobbink, R., Hicks, K., Galloway, J., Spranger, T., Alkemade, R., Ashmore, M., Bustamante, M., Cinderby, S., Davidson, E., Dentener, F., Emmett, B., Erisman, J. W., Fenn, M., Gilliam, F., Nordin, A., Pardo, L., and De Vries, W.: Global assessment of nitrogen deposition effects on terrestrial plant diversity: a synthesis, Ecol. Appl., 20, 30-59, 10.1890/08-1140.1, 2010.

Bouwman, A. F., Van Vuuren, D. P., Derwent, R. G., and Posch, M.: A global analysis of acidification and eutrophication of terrestrial ecosystems, Water Air and Soil Pollution, 141, 349-382, 10.1023/a:1021398008726, 2002.

Cao, J., Garbaccio, R., and Ho, M. S.: China's 11th Five-Year Plan and the Environment: Reducing SO2 Emissions, Rev Env Econ Policy, 3, 231-250, 10.1093/reep/rep006, 2009.

Dentener, F., Drevet, J., Lamarque, J. F., Bey, I., Eickhout, B., Fiore, A. M., Hauglustaine, D., Horowitz, L. W., Krol, M., Kulshrestha, U. C., Lawrence, M., Galy-Lacaux, C., Rast, S., Shindell, D., Stevenson, D., Van Noije, T., Atherton, C., Bell, N., Bergman, D., Butler, T., Cofala, J., Collins, B., Doherty, R., Ellingsen, K., Galloway, J., Gauss, M., Montanaro, V., Muller, J. F., Pitari, G., Rodriguez, J., Sanderson, M., Solmon, F., Strahan, S., Schultz, M., Sudo, K., Szopa, S., and Wild, O.: Nitrogen and sulfur deposition on regional and global scales: A multimodel evaluation, Global Biogeochem Cy, 20, 21, 10.1029/2005gb002672, 2006.

Doney, S. C., Mahowald, N., Lima, I., Feely, R. A., Mackenzie, F. T., Lamarque, J. F., and Rasch, P. J.: Impact of anthropogenic atmospheric nitrogen and sulfur deposition on ocean acidification and the inorganic carbon system, Proceedings of the National Academy of Sciences of the United States of America, 104, 14580-14585, 10.1073/pnas.0702218104, 2007.

Du, E. Z., de Vries, W., Galloway, J. N., Hu, X. Y., and Fang, J. Y.: Changes in wet nitrogen deposition in the United States between 1985 and 2012, Environ Res Lett, 9, 2014.

Duce, R. A., LaRoche, J., Altieri, K., Arrigo, K. R., Baker, A. R., Capone, D. G., Cornell, S., Dentener, F., Galloway, J., Ganeshram, R. S., Geider, R. J., Jickells, T., Kuypers, M. M., Langlois, R., Liss, P. S., Liu, S. M., Middelburg, J. J., Moore, C. M., Nickovic, S., Oschlies, A., Pedersen, T., Prospero, J., Schlitzer, R., Seitzinger, S., Sorensen, L. L., Uematsu, M., Ulloa, O., Voss, M., Ward, B., and Zamora, L.: Impacts of atmospheric anthropogenic nitrogen on the open ocean, Science, 320, 893-897, 10.1126/science.1150369, 2008.

Galloway, J. N., Townsend, A. R., Erisman, J. W., Bekunda, M., Cai, Z. C., Freney, J. R., Martinelli, L. A., Seitzinger, S. P., and Sutton, M. A.: Transformation of the nitrogen cycle: Recent trends, questions, and potential solutions, Science, 320, 889-892, 10.1126/science.1136674, 2008.

Galmarini, S., Koffi, B., Solazzo, E., Keating, T., Hogrefe, C., Schulz, M., Benedictow, A., Griesfeller, J. J., Janssens-Maenhout, G., Carmichael, G., Fu, J., and Dentener, F.: Technical note: Coordination and harmonization of the multi-scale, multi-model activities HTAP2, AQMEII3, and MICS-Asia3: simulations, emission inventories, boundary conditions, and model output formats, Atmos. Chem. Phys., 17, 1543-1555, 10.5194/acp-17-1543-2017, 2017.

Holland, E. A., Braswell, B. H., Lamarque, J. F., Townsend, A., Sulzman, J., Muller, J. F., Dentener, F., Brasseur, G., Levy, H., Penner, J. E., and Roelofs, G. J.: Variations in the predicted spatial distribution of atmospheric nitrogen deposition and their impact on carbon uptake by terrestrial ecosystems, J Geophys Res-Atmos, 102, 15849-15866, 10.1029/96jd03164, 1997.

Hemispheric Transport of Air Pollution (HTAP): Hemispheric Transport of Air Pollution 2010. Part A: Ozone and Particulate Matter, Air Pollution Studies No. 17, edited by: Dentener, F., Keating, T., and Akimoto, H., United Nations, New York, USA, 2010.

Huang, M., Carmichael, G. R., Pierce, R. B., Jo, D. S., Park, R. J., Flemming, J., Emmons, L. K., Bowman, K. W., Henze, D. K., Davila, Y., Sudo, K., Jonson, J. E., Tronstad Lund, M., Janssens-Maenhout, G., Dentener, F. J., Keating, T. J., Oetjen, H., and Payne, V. H.: Impact of intercontinental pollution transport on North American ozone air pollution: an HTAP phase 2 multi-model study, Atmos. Chem. Phys., 17, 5721-5750, 10.5194/acp-17-5721-2017, 2017

Janssens-Maenhout, G., Crippa, M., Guizzardi, D., Dentener, F., Muntean, M., Pouliot, G., Keating, T., Zhang, Q., Kurokawa, J., Wankmüller, R., Denier van der Gon, H., Kuenen, J. J. P., Klimont, Z., Frost, G., Darras, S., Koffi, B., and Li, M.: HTAP_v2.2: a mosaic of regional and global emission grid maps for 2008 and 2010 to study hemispheric transport of air pollution, Atmos. Chem. Phys., 15, 11411-11432, 10.5194/acp-15-11411-2015, 2015.

Janssens, I. A., Dieleman, W., Luyssaert, S., Subke, J. A., Reichstein, M., Ceulemans, R., Ciais, P., Dolman, A. J., Grace, J., Matteucci, G., Papale, D., Piao, S. L., Schulze, E. D., Tang, J., and Law, B. E.: Reduction of forest soil respiration in response to nitrogen deposition, Nature Geoscience, 3, 315-322, 10.1038/ngeo844, 2010.

Jia, Y., Yu, G., Gao, Y., He, N., Wang, Q., Jiao, C., and Zuo, Y.: Global inorganic nitrogen dry deposition inferred from ground- and space-based measurements, Scientific reports, 6, 19810, 10.1038/srep19810, 2016.

Jickells, T.: The role of air-sea exchange in the marine nitrogen cycle, Biogeosciences, 3, 271-280, 2006.

Jickells, T. D., Buitenhuis, E., Altieri, K., Baker, A. R., Capone, D., Duce, R. A., Dentener, F., Fennel, K., Kanakidou, M., LaRoche, J., Lee, K., Liss, P., Middelburg, J. J., Moore, J. K., Okin, G., Oschlies, A., Sarin, M., Seitzinger, S., Sharples, J., Singh, A., Suntharalingam, P., Uematsu, M., and Zamora, L. M.: A reevaluation of the magnitude and impacts of anthropogenic atmospheric nitrogen inputs on the ocean, Global Biogeochem Cy, 31, 289-305, 2017.

Jonson, J. E., Schulz, M., Emmons, L., Flemming, J., Henze, D., Sudo, K., Tronstad Lund, M., Lin, M., Benedictow, A., Koffi, B., Dentener, F., Keating, T., and Kivi, R.: The effects of intercontinental emission sources on European air pollution levels, Atmos. Chem. Phys. Discuss., 2018, 1-26, 10.5194/acp-2018-79, 2018.

Kanakidou, M., Myriokefalitakis, S., Daskalakis, N., Fanourgakis, G., Nenes, A., Baker, A. R., Tsigaridis, K., and Mihalopoulos, N.: Past, Present, and Future Atmospheric Nitrogen Deposition, Journal of the Atmospheric Sciences, 73, 2039-2047, 10.1175/jas-d-15-0278.1, 2016.

Kim, S. W., Heckel, A., McKeen, S. A., Frost, G. J., Hsie, E. Y., Trainer, M. K., Richter, A., Burrows, J. P., Peckham, S. E., and Grell, G. A.: Satellite-observed U.S. power plant NOxemission reductions and their impact on air quality, Geophys Res Lett, 33, 10.1029/2006gl027749, 2006.

Kurokawa, J., Ohara, T., Morikawa, T., Hanayama, S., Janssens-Maenhout, G., Fukui, T., Kawashima, K., and Akimoto, H.: Emissions of air pollutants and greenhouse gases over Asian regions during 2000-2008: Regional Emission inventory in ASia (REAS) version 2, Atmospheric Chemistry and Physics, 13, 11019-11058, 10.5194/acp-13-11019-2013, 2013.

Lamarque, J. F., Kiehl, J. T., Brasseur, G. P., Butler, T., Cameron-Smith, P., Collins, W. D., Collins, W. J., Granier, C., Hauglustaine, D., Hess, P. G., Holland, E. A., Horowitz, L., Lawrence, M. G., McKenna, D., Merilees, P., Prather, M. J., Rasch, P. J., Rotman, D., Shindell, D., and Thornton, P.: Assessing future nitrogen deposition and carbon cycle feedback using a multimodel approach: Analysis of nitrogen deposition, J Geophys Res-Atmos, 110, 10.1029/2005jd005825, 2005.

Lamarque, J. F., Dentener, F., McConnell, J., Ro, C. U., Shaw, M., Vet, R., Bergmann, D., Cameron-Smith, P., Dalsoren, S., Doherty, R., Faluvegi, G., Ghan, S. J., Josse, B., Lee, Y. H., MacKenzie, I. A., Plummer, D., Shindell, D. T., Skeie, R. B., Stevenson, D. S., Strode, S., Zeng, G., Curran, M., Dahl-Jensen, D., Das, S., Fritzsche, D., and Nolan, M.: Multi-model mean nitrogen and sulfur deposition from the Atmospheric Chemistry and Climate Model Intercomparison Project (ACCMIP): evaluation of historical and projected future changes, Atmospheric Chemistry and Physics, 13, 7997-8018, 10.5194/acp-13-7997-2013, 2013.

Li, M., Zhang, Q., Kurokawa, J., Woo, J. H., He, K. B., Lu, Z. F., Ohara, T., Song, Y., Streets, D. G., Carmichael, G. R., Cheng, Y. F., Hong, C. P., Huo, H., Jiang, X. J., Kang, S. C., Liu, F., Su, H., and Zheng, B.: MIX: a mosaic Asian anthropogenic emission inventory under the international collaboration framework of the MICS-Asia and HTAP, Atmospheric Chemistry and Physics, 17, 935-963, 2017.

Li, Y., Schichtel, B. A., Walker, J. T., Schwede, D. B., Chen, X., Lehmann, C. M. B., Puchalski, M. A., Gay, D. A., and Collett, J. L.: Increasing importance of deposition of reduced nitrogen in the United States, Proceedings of the National Academy of Sciences of the United States of America, 113, 5874-5879, 10.1073/pnas.1525736113, 2016.

Lloret, J., and Valiela, I.: Unprecedented decrease in deposition of nitrogen oxides over North America: the relative effects of emission controls and prevailing air-mass trajectories, Biogeochemistry, 129, 165-180, 10.1007/s10533-016-0225-5, 2016.

Lu, Z., Streets, D. G., Zhang, Q., Wang, S., Carmichael, G. R., Cheng, Y. F., Wei, C., Chin, M., Diehl, T., and Tan, Q.: Sulfur dioxide emissions in China and sulfur trends in East Asia since 2000, Atmospheric Chemistry and Physics, 10, 6311-6331, 2010.

Moxim, W. J., Levy, H., and Kasibhatla, P. S.: Simulated global tropospheric PAN: Its transport and impact on NOx, J Geophys Res-Atmos, 101, 12621-12638, 10.1029/96jd00338, 1996.

Reay, D. S., Dentener, F., Smith, P., Grace, J., and Feely, R. A.: Global nitrogen deposition and carbon sinks, Nature Geoscience, 1, 430-437, 10.1038/ngeo230, 2008.

Richter, A., Burrows, J. P., Nuss, H., Granier, C., and Niemeier, U.: Increase in tropospheric nitrogen dioxide over China observed from space, Nature, 437, 129-132, 10.1038/nature04092, 2005.

Sanderson, M. G., Collins, W. J., Johnson, C. E., and Derwent, R. G.: Present and future acid deposition to ecosystems: The effect of climate change, Atmospheric Environment, 40, 1275-1283, 10.1016/j.atmosenv.2005.10.031, 2006.

Sanderson, M. G., Dentener, F. J., Fiore, A. M., Cuvelier, C., Keating, T. J., Zuber, A., Atherton, C. S., Bergmann, D. J., Diehl, T., Doherty, R. M., Duncan, B. N., Hess, P., Horowitz, L. W., Jacob, D. J., Jonson, J. E., Kaminski, J. W., Lupu, A., MacKenzie, I. A., Mancini, E., Marmer, E., Park, R., Pitari, G., Prather, M. J., Pringle, K. J., Schroeder, S., Schultz, M. G., Shindell, D. T., Szopa, S., Wild, O.,

and Wind, P.: A multi-model study of the hemispheric transport and deposition of oxidised nitrogen, Geophys Res Lett, 35, 10.1029/2008gl035389, 2008.

Schwede, D., Zhang, L. M., Vet, R., and Lear, G.: An intercomparison of the deposition models used in the CASTNET and CAPMoN networks, Atmospheric Environment, 45, 1337-1346, 2011.

Shen, J., Chen, D., Bai, M., Sun, J., Coates, T., Lam, S. K., and Li, Y.: Ammonia deposition in the neighbourhood of an intensive cattle feedlot in Victoria, Australia, Scientific reports, 6, 32793, 10.1038/srep32793, 2016.

Sickles, J. E., and Shadwick, D. S.: Comparison of particulate sulfate and nitrate at collocated CASTNET and IMPROVE sites in the eastern US, Atmospheric Environment, 42, 2062-2073, 2008.

Stjern, C. W., Samset, B. H., Myhre, G., Bian, H., Chin, M., Davila, Y., Dentener, F., Emmons, L., Flemming, J., Haslerud, A. S., Henze, D., Jonson, J. E., Kucsera, T., Lund, M. T., Schulz, M., Sudo, K., Takemura, T., and Tilmes, S.: Global and regional radiative forcing from 20 % reductions in BC, OC and SO4 – an HTAP2 multi-model study, Atmos. Chem. Phys., 16, 13579-13599, 10.5194/acp-16-13579-2016, 2016.

Sun, J., Fu, J. S., and Huang, K.: Organic nitrates and other oxidized nitrogen compounds contribute significantly to the total nitrogen depositions in the United States, Proceedings of the National Academy of Sciences of the United States of America, 113, E4433-E4434, 2016.

Sun, J., Fu, J. S., Lynch, J. A., Huang, K., and Gao, Y.: Climate-driven exceedance of total (wet plus dry) nitrogen (N) plus sulfur (S) deposition to forest soil over the conterminous US, Earths Future, 5, 560-576, 2017.

Tan, J. N., Fu, J. S., Huang, K., Yang, C. E., Zhuang, G. S., and Sun, J.: Effectiveness of SO2 emission control policy on power plants in the Yangtze River Delta, China-post-assessment of the 11th Five-Year Plan, Environmental Science and Pollution Research, 24, 8243-8255, 2017.

Tan, J., Fu, J. S., Dentener, F., Sun, J., Emmons, L., Tilmes, S., Flemming, J., Takemura, T., Bian, H., Zhu, Q., Yang, C. E., and Keating, T.: Source contributions of sulfur and nitrogen deposition - an HTAP II multi model study on hemispheric transport, Atmos. Chem. Phys. Discuss., 2018, 1-31, 10.5194/acp-2018-109, 2018.

Tørseth, K., Aas, W., Breivik, K., Fjæraa, A. M., Fiebig, M., Hjellbrekke, A. G., Lund Myhre, C., Solberg, S., and Yttri, K. E.: Introduction to the European Monitoring and Evaluation Programme (EMEP) and observed atmospheric composition change during 1972–2009, Atmospheric Chemistry and Physics, 12, 5447-5481, 10.5194/acp-12-5447-2012, 2012.

van der A, R. J., Peters, D. H. M. U., Eskes, H., Boersma, K. F., Van Roozendael, M., De Smedt, I., and Kelder, H. M.: Detection of the trend and seasonal variation in tropospheric NO2over China, Journal of Geophysical Research, 111, 10.1029/2005jd006594, 2006.

van der A, R. J., Eskes, H. J., Boersma, K. F., van Noije, T. P. C., Van Roozendael, M., De Smedt, I., Peters, D. H. M. U., and Meijer, E. W.: Trends, seasonal variability and dominant NOxsource derived from a ten year record of NO2measured from space, Journal of Geophysical Research, 113, 10.1029/2007jd009021, 2008.

Vet, R., Artz, R. S., Carou, S., Shaw, M., Ro, C. U., Aas, W., Baker, A., Bowersox, V. C., Dentener, F., Galy-Lacaux, C., Hou, A., Pienaar, J. J., Gillett, R., Forti, M. C., Gromov, S., Hara, H., Khodzher, T., Mahowald, N. M., Nickovic, S., Rao, P. S. P., and Reid, N. W.: A global assessment of precipitation chemistry and deposition of sulfur, nitrogen, sea salt, base cations, organic acids, acidity and pH, and phosphorus, Atmospheric Environment, 93, 3-100, 10.1016/j.atmosenv.2013.10.060, 2014.

Vitousek, P. M., Aber, J. D., Howarth, R. W., Likens, G. E., Matson, P. A., Schindler, D. W., Schlesinger, W. H., and Tilman, D.: Human alteration of the global nitrogen cycle: Sources and consequences, Ecol. Appl., 7, 737-750, 10.2307/2269431, 1997.

Wesely, M. L.: Parameterization of Surface Resistances to Gaseous Dry Deposition in Regional-Scale Numerical-Models, Atmospheric Environment, 23, 1293-1304, 1989.

Wesely, M. L., and Hicks, B. B.: A review of the current status of knowledge on dry deposition, Atmospheric Environment, 34, 2261-2282, 2000.

Zhang, L., Vet, R., O'Brien, J. M., Mihele, C., Liang, Z., and Wiebe, A.: Dry deposition of individual nitrogen species at eight Canadian rural sites, Journal of Geophysical Research, 114, 10.1029/2008jd010640, 2009a.

Zhang, Q., Streets, D. G., He, K., Wang, Y., Richter, A., Burrows, J. P., Uno, I., Jang, C. J., Chen, D., Yao, Z., and Lei, Y.: NOx emission trends for China, 1995-2004: The view from the ground and the view from space, J Geophys Res-Atmos, 112, 10.1029/2007jd008684, 2007.

Zhang, Q., Streets, D. G., Carmichael, G. R., He, K. B., Huo, H., Kannari, A., Klimont, Z., Park, I. S., Reddy, S., Fu, J. S., Chen, D., Duan, L., Lei, Y., Wang, L. T., and Yao, Z. L.: Asian emissions in 2006 for the NASA INTEX-B mission, Atmospheric Chemistry and Physics, 9, 5131-5153, 2009b.

Figures

Caption:

Fig. 1 Evaluation of MMM performance of SO_4^{2-}, NO_3^- and NH_4^+ wet deposition (mg (N or S) m^{-2} yr^{-1}) at NADP (left), EMEP (middle) and EANET (right) stations. The MMM is the annual wet deposition in 2010 and the observation is 3-year average annual data of 2009-2011. Performances of individual models are in Fig. S2-S4 in the supplementary material.

Fig. 2. Distribution of SO_4^{2-}, NO_3^- and NH_4^+ wet deposition (mg (N or S) m^{-2} yr^{-1}) of MMM and observation. The MMM is the annual wet deposition in 2010 and the observation is 3-year average annual data of 2009-2011.Contours are MMM results and filled circles are observation.

Fig. 3 Evaluation of MMM performance of SO_2, SO_4^{2-}, NO_3^-, HNO_3 and NH_4^+ dry deposition (mg (N or S) m^{-2} yr^{-1}) at CASTNET stations. The MMM is the annual dry deposition in 2010 and the observation data is 3-year average annual data during 2009-2011 from CASTNET network. Performances of individual models are in Fig. S7-S11 in the supplementary material.

Fig. 4. Distribution of SO_2, SO_4^{2-}, NO_3^-, HNO_3 and NH_4^+ dry deposition (mg (N or S) m^{-2} yr^{-1}) of MMM and observation. The MMM is the annual dry deposition in 2010 and the observation is 3-year average annual data of 2009-2011. Contours are MMM results and filled circles are inferential data from CASTNET.

Fig. 5 (top panel) MMM results of S emission and deposition in 2010 (mg(S) m^{-2} yr^{-1}) and ratio of S deposition in S emission (%). (bottom panel) MMM results of S dry and wet deposition in 2010 (mg(S) m^{-2} yr^{-1}) and ratio of dry deposition in total (wet+dry) deposition (%).

Fig. 6 MMM results of NO_X, NH_3 and N(NO_X + NH_3) emission (mg(N) m^{-2} yr^{-1}) (left panel), NO_y, NH_X and N (NO_y+NH_X) deposition (mg(N) m^{-2} yr^{-1}) in 2010. (middel panel), ratio of NO_y, NH_X and N deposition to NO_X, NH_3 and N(NO_X + NH_3) emission (%) (right panel). purple colors represent regions where deposition is larger than emission.

Fig. 7 (top panel) The percentage of dry deposition in wet+dry deposition for NO_y, NH_x and N (NO_y+NH_x) deposition. The ratio is calculated as (dry deposition)/ (dry+wet deposition) ×100%. (bottom panel) The percentage of NHx deposition in N (NO_y+NH_x) deposition for wet, dry and (wet+dry) deposition. The ratio is calculated as (NH_x deposition)/ (NO_y+NH_x deposition).

Fig. 1

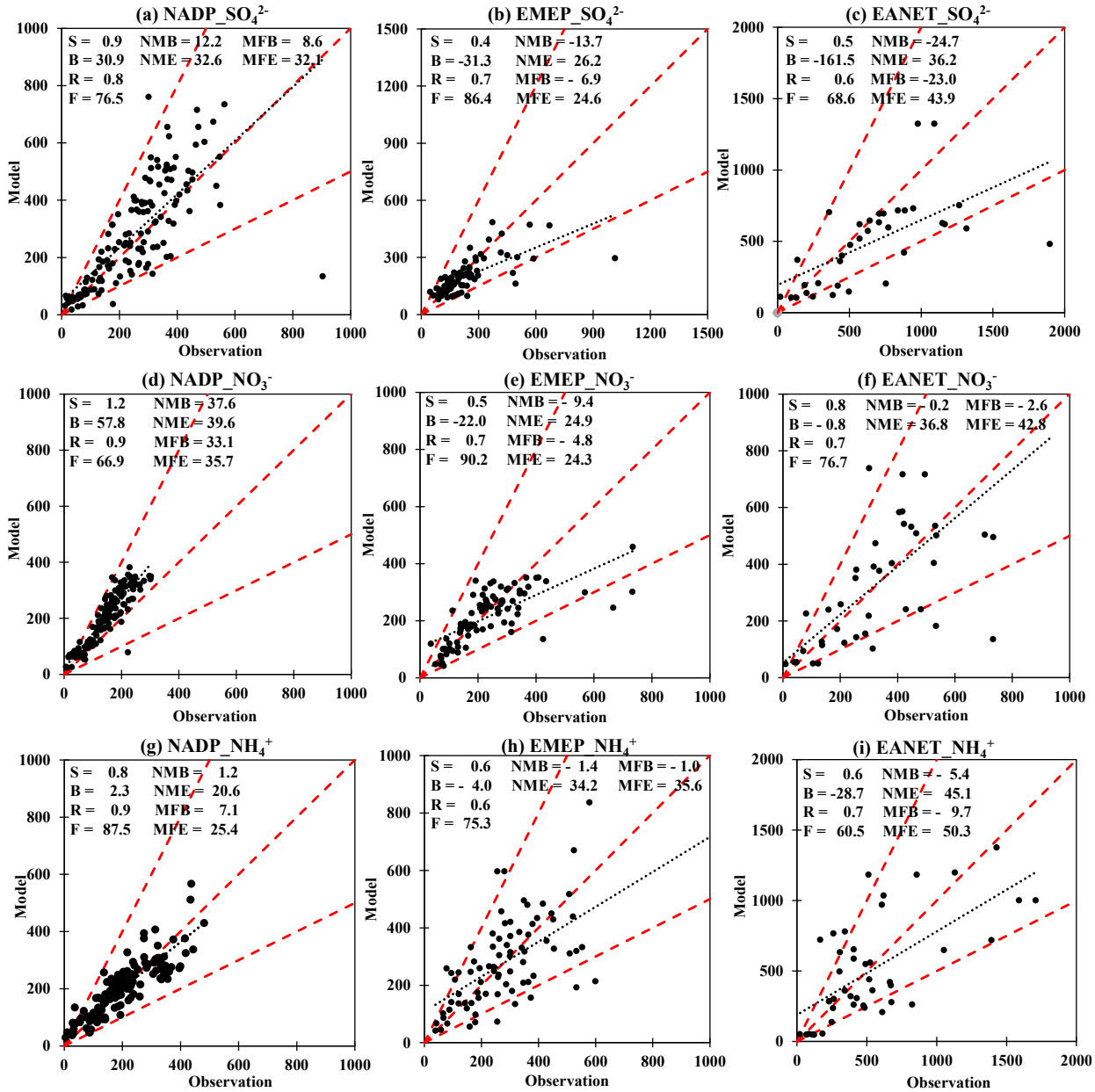

Fig. 1 Evaluation of MMM performance of SO_4^{2-}, NO_3^- and NH_4^+ wet deposition (mg (N or S) m^{-2} yr^{-1}) at NADP (left), EMEP (middle) and EANET (right) stations. The MMM is the annual wet deposition in 2010 and the observation is 3-year average annual data of 2009-2011. Performances of individual models are in Fig. S2-S4 in the supplementary material.

Fig. 2

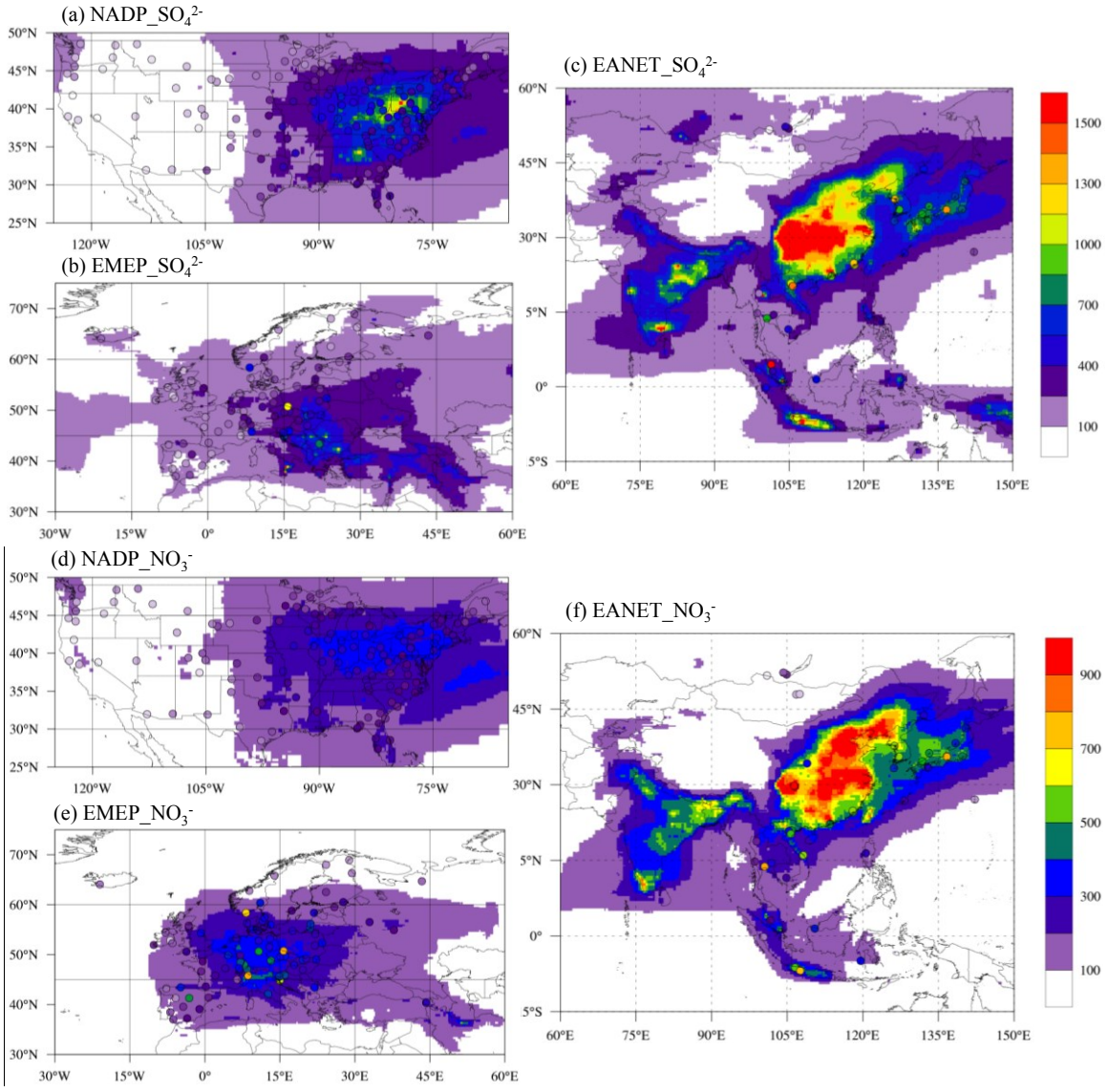
(a) NADP_SO4 2-
(b) EMEP_SO4 2-
(c) EANET_SO4 2-
(d) NADP_NO3 -
(e) EMEP_NO3 -
(f) EANET_NO3 -
1500
1300
1000
700
400
100
900
700
500
300
100

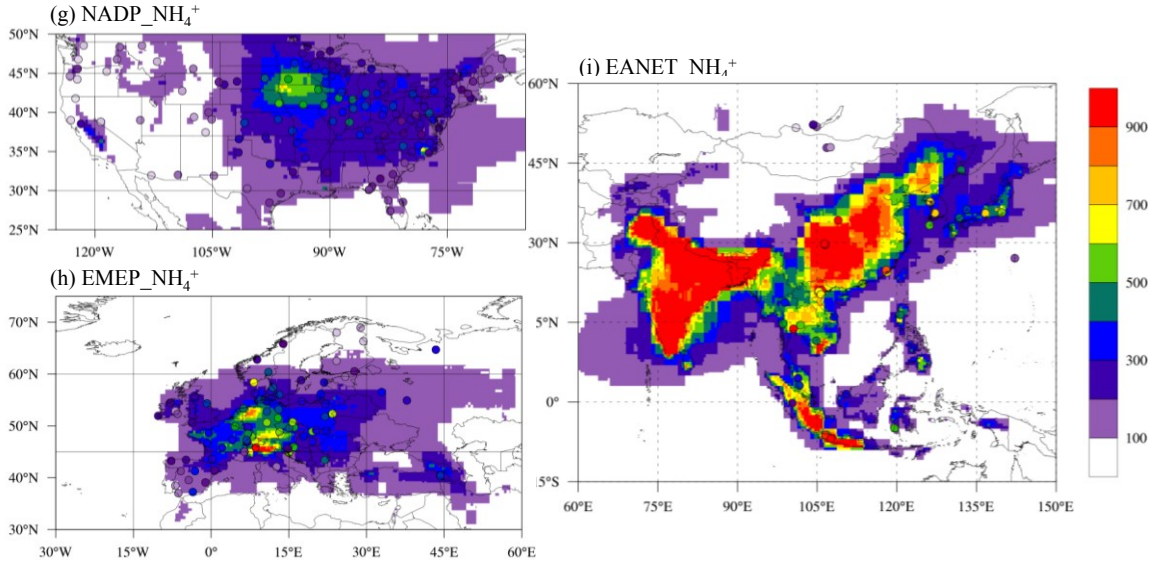

Fig. 2. Distribution of SO_4^{2-}, NO_3^- and NH_4^+ wet deposition (mg (N or S) m^{-2} yr^{-1}) of MMM and observation. The MMM is the annual wet deposition in 2010 and the observation is 3-year average annual data of 2009-2011.Contours are MMM results and filled circles are observation.

Fig. 3

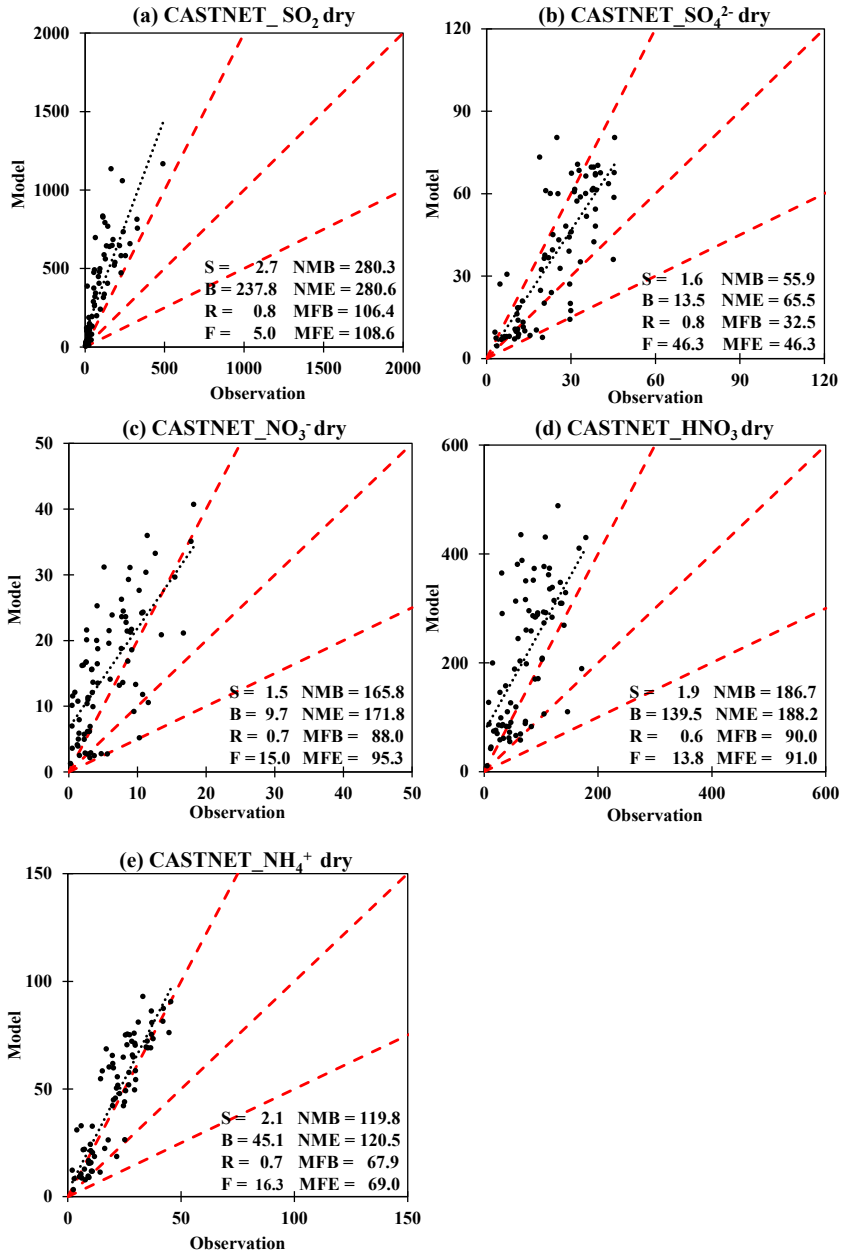

Fig. 3 Evaluation of MMM performance of SO_2, SO_4^{2-}, NO_3^-, HNO_3 and NH_4^+ dry deposition (mg (N or S) m^{-2} yr^{-1}) at CASTNET stations. The MMM is the annual dry deposition in 2010 and the observation data is 3-year average annual data during 2009-2011 from CASTNET network. Performances of individual models are in Fig. S7-S11 in the supplementary material.

Fig. 4

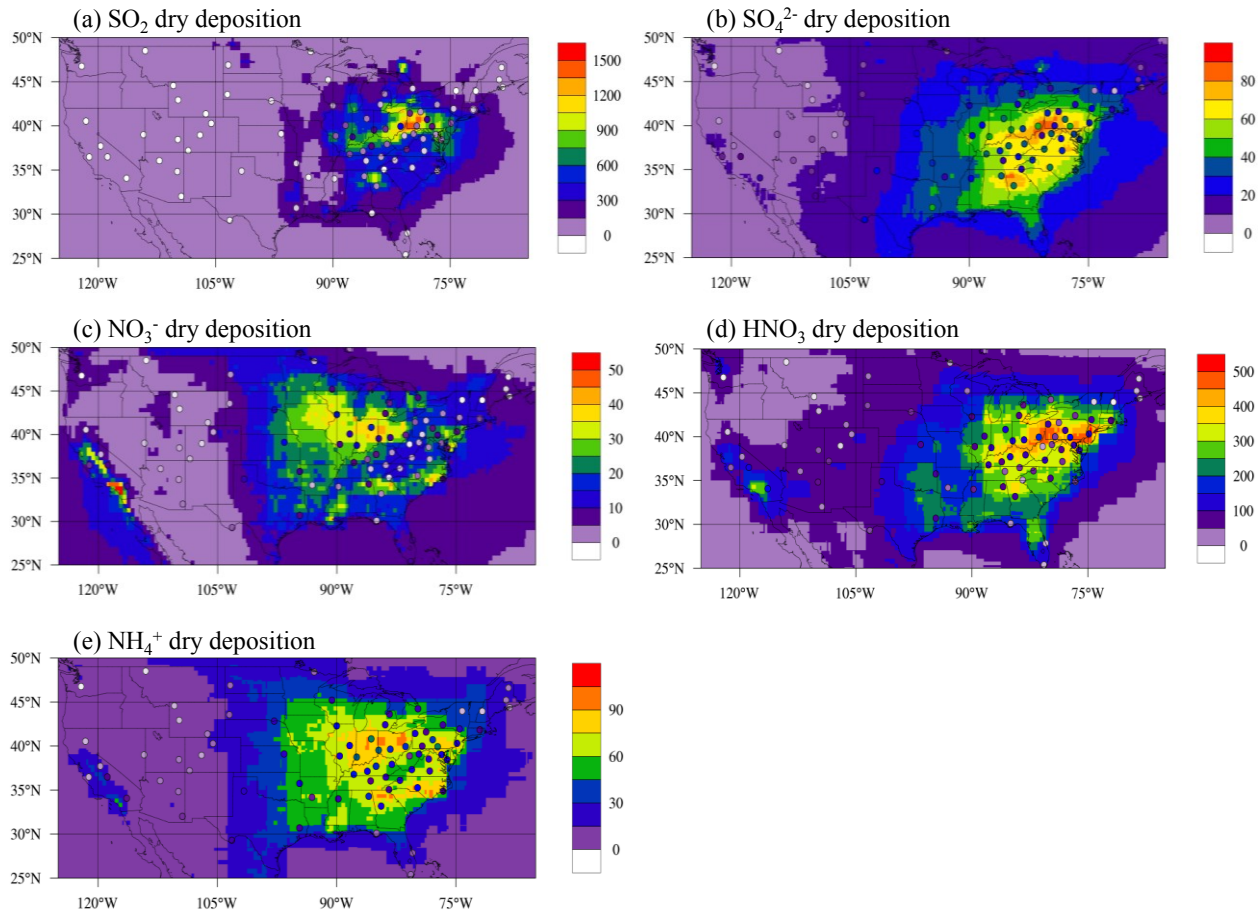

Fig. 4. Distribution of SO_2, SO_4^{2-}, NO_3^-, HNO_3 and NH_4^+ dry deposition (mg (N or S) m^{-2} yr^{-1}) of MMM and observation. The MMM is the annual dry deposition in 2010 and the observation is 3-year average annual data of 2009-2011. Contours are MMM results and filled circles are inferential data from CASTNET.

Fig. 5

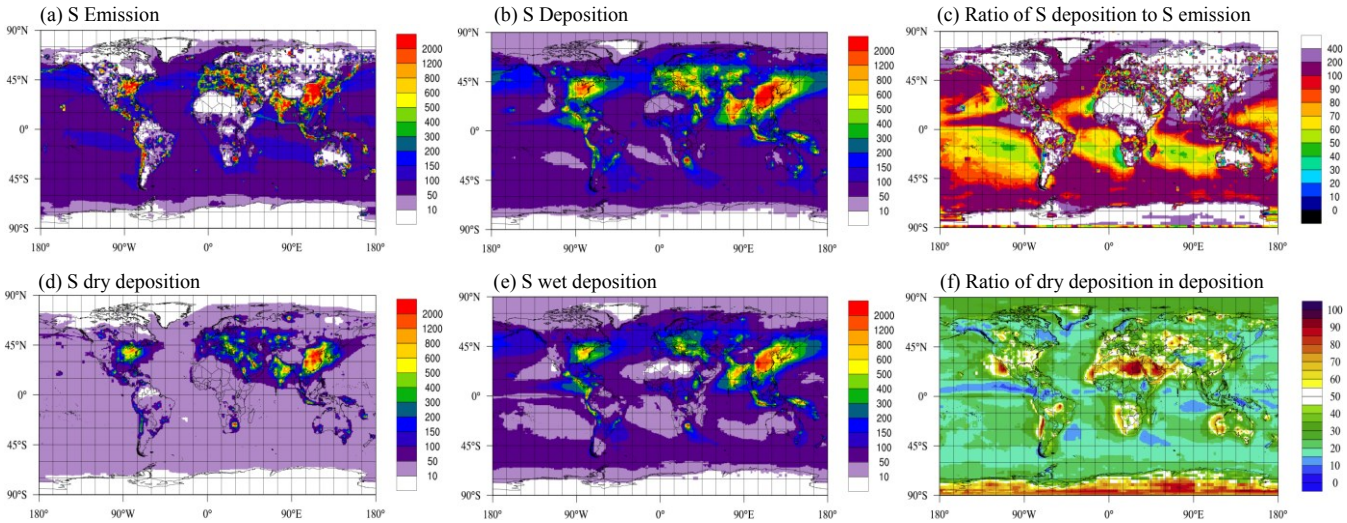

Fig. 5 (top panel) MMM results of S emission and deposition in 2010 (mg(S) m^{-2} yr^{-1}) and ratio of S deposition in S emission (%). (bottom panel) MMM results of S dry and wet deposition in 2010 (mg(S) m^{-2} yr^{-1}) and ratio of dry deposition in total (wet+dry) deposition (%).

Fig. 6

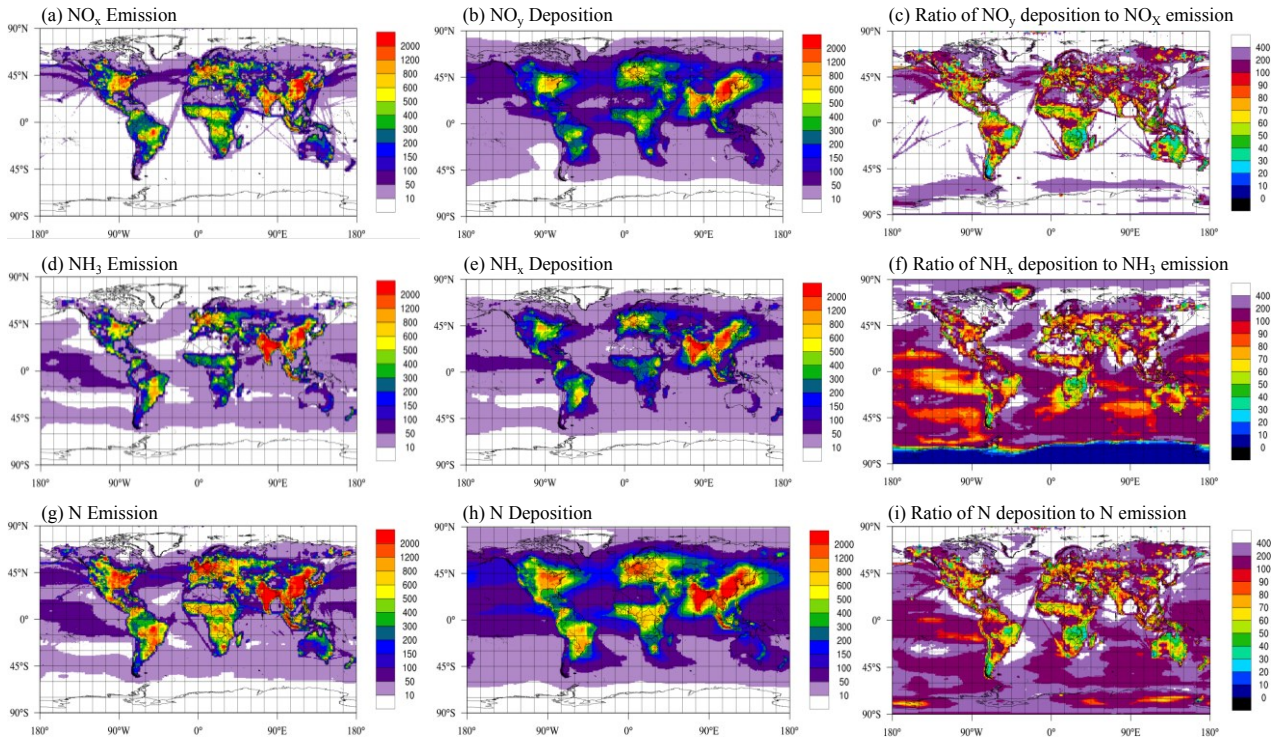

Fig. 6 MMM results of NO_X, NH_3 and $N(NO_X + NH_3)$ emission (mg(N) m^{-2} yr^{-1}) (left panel), NO_y, NH_X and N (NO_y+NH_X) deposition (mg(N) m^{-2} yr^{-1}) in 2010. (middel panel), ratio of NO_y, NH_X and N deposition to NO_X, NH_3 and $N(NO_X + NH_3)$ emission (%) (right panel). purple colors represent regions where deposition is larger than emission.

Fig. 7

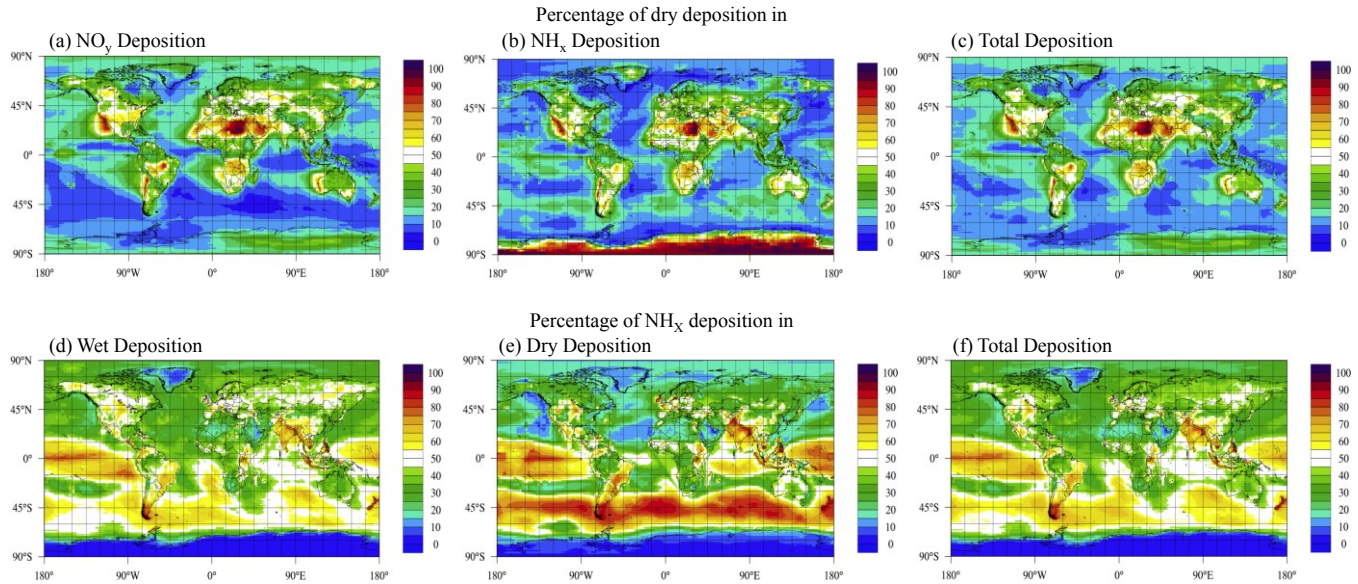

Fig. 7 (top panel) The percentage of dry deposition in wet+dry deposition for NO_y, NH_x and N (NO_y+NH_x) deposition. The ratio is calculated as (dry deposition)/ (dry+wet deposition) ×100%. (bottom panel) The percentage of NH_x deposition in N (NO_y+NH_x) deposition for wet, dry and (wet+dry) deposition. The ratio is calculated as (NH_x deposition)/ (NO_y+NH_x deposition).

Tables

Table 1. Intercomparison of HTAP II MMM performance with previous projects on wet deposition. The unit is mg (N or S) m^{-2} yr^{-1}.

Wet SO_4^{2-} Deposition	North America				Europe				Asia			
	PhotoComp	HTAP I	ACCMIP	HTAP II	PhotoComp	HTAP I	ACCMIP	HTAP II	PhotoComp	HTAP I	ACCMIP	HTAP II
Linear Fit Slope	0.9	1	0.6	0.9	0.4	0.6	0.3	0.4	0.4	0.5	0.3	0.5
Mean Bias	46.3	50	-18.8	30.9	-67.1	51.5	-125.3	-31.3	-218.6	-182.1	-292.4	-161.5
Mean Observation	309.8	309.8	309.8	253.7	404.5	404.5	404.5	228.7	686.1	686.1	686.1	653.7
Mean Model	356.1	359.8	291	284.6	337.3	456.1	279.3	197.4	467.5	504.1	393.7	492.2
R	0.9	0.9	0.9	0.8	0.6	0.6	0.6	0.7	0.9	0.9	0.8	0.6
Fraction within ±50%	70.4	70	72.2	76.5	78.7	52.8	78.7	86.4	80	88	72	68.6
Number of stations	346	346	346	136	126	126	126	82	49	49	49	43

Wet NO_3^- Deposition	North America				Europe				Asia			
	PhotoComp	HTAP I	ACCMIP	HTAP II	PhotoComp	HTAP I	ACCMIP	HTAP II	PhotoComp	HTAP I	ACCMIP	HTAP II
Linear Fit Slope	1	1	0.9	1.2	0.3	0.3	0.3	0.5	0.5	0.5	0.4	0.8
Mean Bias	34.8	21.9	44.3	57.8	-41.4	-60	-75.2	-22.0	-47.8	-49.3	-46.4	-0.8
Mean Observation	191.3	191.3	191.3	153.7	300.5	300.5	300.5	237.3	263	263	263	356.4
Mean Model	226.1	213.3	235.6	211.5	259.1	240.5	225.3	215.4	215.2	213.7	216.7	355.7
R	0.8	0.9	0.9	0.9	0.6	0.6	0.6	0.7	0.8	0.8	0.8	0.7
Fraction within ±50%	77	84.3	68.7	66.9	75	85.2	85.2	90.2	84	84	88	76.7
Number of stations	346	346	346	136	126	126	126	82	49	49	49	43

Wet NH_4^+ Deposition	North America				Europe				Asia			
	PhotoComp	HTAP I	ACCMIP	HTAP II	PhotoComp	HTAP I	ACCMIP	HTAP II	PhotoComp	HTAP I	ACCMIP	HTAP II
Linear Fit Slope	0.8	0.9	0.5	0.8	0.4	0.4	0.3	0.6	0.8	0.7	0.1	0.6
Mean Bias	5.5	10.9	-12.1	2.3	-23.9	-49.7	-94.7	-4.0	-69.7	-63.4	-136.2	-28.7
Mean Observation	161.3	161.3	161.3	195.5	336	336	336	286.1	400.5	400.5	400.5	534.5
Mean Model	166.8	172.2	149.2	197.9	312.1	286.4	241.3	282.2	330.8	337.1	264.4	505.8
R	0.9	0.9	0.8	0.9	0.8	0.6	0.6	0.6	0.8	0.8	0.2	0.7
Fraction within ±50%	82.2	84.8	75.7	87.5	73.9	79.5	78.4	75.3	76	68	56	60.5
Number of stations	346	346	346	136	126	126	126	82	49	49	49	43

Table 2. Intercomparison of HTAP II MMM performance with previous project on dry deposition. The unit is mg (N or S) m^{-2} yr^{-1}. S dry deposition is the sum of SO_2 and SO_4^{2-} dry deposition. N dry deposition is the sum of HNO_3, NO_3^- and NH_4^+ dry deposition (not include NO_2 and NH_3 deposition).

	S dry deposition			SO_2 dry deposition			SO_4^{2-} dry deposition		
	ACCMIP	HTAP I	HTAP II	ACCMIP	HTAP I	HTAP II	ACCMIP	HTAP I	HTAP II
Linear fit slope	1	-	2.7	1	-	2.7	1	-	1.6
Mean Bias	280.9	367	251.2	264	-	237.8	17	-	13.5
Mean observation	225.6	-	108.9	191	-	84.8	35	-	24.1
Mean model	506.5	-	360.2	455	-	322.6	52	-	37.5
R	0.8	0.8	0.8	0.8	-	0.8	0.9	-	0.8
Fraction within ±50%	6	-	12.5	6	-	5	48	-	46.3

	N dry deposition			HNO_3 dry deposition			NH_4^+ dry deposition		
	ACCMIP	HTAP I	HTAP II	ACCMIP	HTAP I	HTAP II	ACCMIP	HTAP I	HTAP II
Linear fit slope	-	-	2.1	1	-	1.9	2	-	2.1
Mean Bias	-	411 (eastern NA) 114 (western NA)	185.1	75	-	139.5	33	-	24.6
Mean observation	-	-	101.1	119	-	74.7	28	-	20.5
Mean model	-	-	286.1	195	-	214.2	60	-	45.1
R	-	0.8	0.7	0.8	-	0.6	0.8	-	0.7
Fraction within ±50%	-	-	13.8	38	-	13.8	18	-	16.3

Table 3. MMM estimates of S deposition and emission in 2010 (Tg(S) yr^{-1}) and comparison with HTAP I results. Δ is the difference between 2010 and 2001 calculated as (HTAP II – HTAP I). The number in parentheses is the percentage of change, calculated as $\frac{(\text{HTAP II} - \text{HTAP I})}{\text{HTAP I}} \times 100\%$.

Regions	S emission						S deposition					
	Non-coastal			Coastal			Non-coastal			Coastal		
	HTAP II (2010)	HTAP I (2001)	Δ	HTAP II (2010)	HTAP I (2001)	Δ	HTAP II (2010)	HTAP I (2001)	Δ	HTAP II (2010)	HTAP I (2001)	Δ
3. North America	6.2	9.5	-3.3 (-34.3)	1.0	1.3	-0.2 (-19.2)	4.7	7.2	-2.5 (-34.8)	1.3	1.3	0.0 (-1.2)
4. Europe	3.9	10.0	-6.1 (-60.8)	1.6	3.6	-1.9 (-54.2)	2.7	6.4	-3.7 (-58.2)	1.5	2.9	-1.4 (-49.6)
5. South Asia	5.2	3.3	1.9 (56.4)	0.8	0.8	0.0 (-3.6)	3.7	2.4	1.4 (57.8)	1.0	0.9	0.1 (17.0)
6. East Asia	15.0	15.6	-0.6 (-4.0)	1.8	3.2	-1.4 (-42.8)	11.2	11.9	-0.7 (-5.6)	2.9	3.3	-0.4 (-13.3)
7. Southeast Asia	2.5	1.7	0.7 (42.4)	2.6	2.4	0.1 (6.0)	2.4	1.9	0.5 (27.6)	2.8	2.4	0.4 (16.1)
8. Australia	1.5	1.0	0.5 (56.0)	2.0	1.4	0.6 (42.0)	1.0	0.7	0.3 (43.9)	1.5	1.1	0.3 (28.0)
9. North Africa	0.7	1.1	-0.4 (-37.0)	0.9	0.9	0.0 (-2.9)	1.0	1.1	-0.1 (-12.3)	0.5	0.6	-0.1 (-11.3)
10. Sub Saharan Africa	2.5	2.8	-0.4 (-12.6)	0.9	0.7	0.2 (24.2)	2.7	2.6	0.1 (4.8)	0.7	0.7	0.0 (-4.9)
11. Middle East	3.2	1.9	1.3 (68.9)	1.1	0.5	0.6 (108.1)	1.7	1.2	0.5 (47.0)	0.6	0.4	0.2 (50.4)
12. Central America	2.2	2.1	0.2 (7.7)	1.4	1.7	-0.3 (-15.2)	1.4	1.4	0.0 (1.6)	1.4	1.4	0.0 (2.0)
13. South America	3.1	2.7	0.4 (16.9)	0.8	1.0	-0.2 (-23.3)	2.4	2.1	0.3 (14.3)	0.6	0.6	0.0 (1.6)
14. RBU	2.9	5.1	-2.2 (-43.9)	0.5	0.5	0.0 (-5.8)	3.6	5.3	-1.7 (-32.1)	0.9	0.8	0.1 (9.7)
15. Central Asia	1.6	1.4	0.2 (18.3)	0.0	0.0	0.0 (-5.9)	1.2	1.2	0.0 (2.7)	0.1	0.1	0.0 (-13.5)
17. Antarctic	1.1	1.1	-0.1 (-7.2)	0.0	0.0	0.0 (0)	1.4	0.8	0.6 (73.7)	0.0	0.0	0.0 (0)
Continental	51.5	59.3	-7.7 (-13.1)	15.3	18.0	-2.7 (-14.8)	41.0	46.0	-4.9 (-10.7)	15.6	16.5	-0.8 (-5.1)
2. Ocean	23.9	18.1	5.8 (31.9)				26.9	23.3	3.6 (15.5)			
1. World Total	75.4	77.4	-2.0 (-2.6)	15.3	18.0	-2.7 (-14.8)	67.9	69.2	-1.3 (-1.9)	15.6	16.5	-0.8 (-5.1)

Table 4. MMM estimates of N, NO_y and NH_X deposition and emission in 2010 (Tg(N) yr^{-1}) . The number in the parenthesis is the percentage in world total emission/deposition.

Regions	NO_X emission		NO_y deposition		NH_3 emission		NH_X deposition		N emission		N deposition	
	Non-coastal	Coastal	Non-coastal	Coastal	Non-coastal	Coastal	Non-coastal	Coastal	Non-coastal	Coastal	Non-coastal	Coastal
3. North America	6.6 (10.9)	0.6 (1.1)	4.4 (7.5)	0.8 (1.4)	3.7 (6.9)	0.2 (0.3)	3.4 (6.3)	0.4 (0.7)	10.3 (9.0)	0.8 (0.7)	7.8 (6.9)	1.2 (1.0)
4. Europe	3.7 (6.2)	1.2 (1.9)	2.6 (4.4)	1.2 (2.1)	3.2 (5.9)	0.6 (1.1)	2.5 (4.6)	0.8 (1.4)	6.9 (6.0)	1.8 (1.6)	5.1 (4.5)	2.0 (1.8)
5. South Asia	4.4 (7.3)	0.4 (0.7)	3.6 (6.0)	0.7 (1.2)	10.4 (19.2)	0.7 (1.3)	8.6 (15.9)	1.0 (1.9)	14.8 (12.9)	1.1 (1.0)	12.1 (10.7)	1.7 (1.5)
6. East Asia	10.1 (16.8)	1.3 (2.1)	8.3 (14.0)	2.2 (3.7)	7.8 (14.4)	0.7 (1.3)	6.7 (12.5)	1.0 (1.9)	18.0 (15.7)	2.0 (1.7)	15.1 (13.3)	3.2 (2.8)
7. Southeast Asia	2.6 (4.4)	1.3 (2.1)	1.9 (3.1)	1.4 (2.3)	3.1 (5.8)	1.5 (2.7)	3.2 (5.9)	1.6 (2.9)	5.8 (5.0)	2.7 (2.4)	5. 1 (4.5)	2.9 (2.6)
8. Australia	1.4 (2.3)	0.3 (0.6)	0.6 (1.0)	0.4 (0.7)	0.7 (1.2)	0.4 (0.8)	0.4 (0.8)	0.4 (0.8)	2.0 (1.8)	0.8 (0.7)	1.0 (0.9)	0.9 (0.8)
9. North Africa	1.5 (2.5)	0.4 (0.7)	1.4 (2.3)	0.4 (0.6)	0.9 (1.7)	0.2 (0.3)	0.7 (1.3)	0.2 (0.3)	2.5 (2.1)	0.6 (0.5)	2.1 (1.9)	0.5 (0.5)
10. Sub Saharan Africa	7.4 (12.2)	0.4 (0.7)	4.7 (7.9)	0.6 (1.1)	4.0 (7.5)	0.3 (0.6)	3.4 (6.4)	0.4 (0.7)	11.4 (10.0)	0.7 (0.6)	8.1 (7.2)	1.0 (0.9)
11. Middle East	1.9 (3.1)	0.5 (0.7)	1.4 (2.4)	0.3 (0.6)	0.7 (1.2)	0.1 (0.2)	0.5 (0.9)	0.1 (0.2)	2.5 (2.2)	0.6 (0.5)	1.9 (1.7)	0.5 (0.4)
12. Central America	2.1 (3.5)	0.8 (1.3)	1.2 (2.1)	0.8 (1.4)	1.4 (2.6)	0.5 (0.9)	1.4 (2.5)	0.6 (1.1)	3.5 (3.1)	1.2 (1.1)	2.6 (2.3)	1.4 (1.3)
13. South America	5.4 (8.9)	0.3 (0.5)	3.4 (5.8)	0.3 (0.5)	4.4 (8.1)	0.3 (0.5)	3.8 (7.1)	0.3 (0.6)	9.8 (8.5)	0.6 (0.5)	7.3 (6.4)	0.6 (0.5)
14. RBU	2.4 (4.1)	0.2 (0.3)	2.4 (4.1)	0.5 (0.9)	1.7 (3.1)	0.1 (0.2)	1.8 (3.4)	0.3 (0.6)	4.1 (3.6)	0.3 (0.2)	4.3 (3.8)	0.8 (0.7)
15. Central Asia	0.7 (1.1)	0.0 (0)	0.6 (1.1)	0.0 (0.1)	0.5 (0.9)	0.0 (0)	0.5 (0.8)	0.0 (0)	1.1 (1.0)	0.0 (0)	1.1 (1.0)	0.1 (0.1)
17. Antarctic	0.0 (0.1)	0.0 (0)	0.1 (0.2)	0.0 (0)	0.0 (0.1)	0.0 (0)	0.1 (0.2)	0.0 (0)	0.1 (0.1)	0.0 (0)	0.2 (0.2)	0.0 (0)
Continental	50.2 (83.2)	7.7 (12.8)	36.7 (61.9)	9.7 (16.4)	42.6 (78.5)	5.6 (10.3)	37.0 (68.6)	7.1 (13.1)	92.9 (81.0)	13.3 (11.6)	73.7 (65.1)	16.8 (14.8)
2. Ocean	2.4 (4)		12.9 (21.7)		6.0 (11.1)		9.9 (18.3)		8.5 (7.4)		22.8 (20.1)	
1. World Total	52.7 (87.2)	7.7 (12.8)	49.6 (83.6)	9.7 (16.4)	48.7 (89.7)	5.6 (10.3)	46.9 (86.9)	7.1 (13.1)	101.3 (88.4)	13.3 (11.6)	96.5 (85.2)	16.8 (14.8)

Table 5. Comparison of N deposition and emission between 2010 (HTAP II) and 2001 (HTAP I) (Tg (N) yr^{-1}). Δ is the difference between 2010 and 2001 calculated as (HTAP II – HTAP I). The numbers in parentheses are the percentage of change, calculated as $\frac{(\text{HTAP II} - \text{HTAP I})}{\text{HTAP I}} \times 100\%$.

Regions	N emission						N deposition					
	Non-coastal			Coastal			Non-coastal			Coastal		
	HTAP II (2010)	HTAP I (2001)	Δ	HTAP II (2010)	HTAP I (2001)	Δ	HTAP II (2010)	HTAP I (2001)	Δ	HTAP II (2010)	HTAP I (2001)	Δ
3. North America	10.3	10.2	0.1 (0.5)	0.8	1.0	-0.2 (-16.8)	7.8	8.1	-0.2 (-3.1)	1.2	1.2	-0.1 (-4.8)
4. Europe	6.9	7.8	-0.9 (-11.8)	1.8	2.7	-0.9 (-33.6)	5.1	5.7	-0.7 (-11.4)	2.0	2.6	-0.6 (-23.6)
5. South Asia	14.8	9.5	5.3 (56.0)	1.1	1.3	-0.2 (-15.5)	12.1	6.7	5.4 (79.7)	1.7	1.7	0.1 (3.8)
6. East Asia	18.0	14.3	3.7 (25.9)	2.0	2.2	-0.2 (-8.1)	15.1	11.9	3.2 (26.8)	3.2	2.6	0.6 (21.9)
7. Southeast Asia	5.8	3.7	2.1 (57.4)	2.7	2.7	0.0 (0.5)	5.1	3.3	1.8 (54.4)	2.9	3.0	0.0 (-0.7)
8. Australia	2.0	2.1	-0.1 (-5.3)	0.8	0.9	-0.2 (-16.6)	1.0	1.3	-0.3 (-23.0)	0.9	1.1	-0.2 (-21.0)
9. North Africa	2.5	2.1	0.3 (15.6)	0.6	0.6	0.1 (9.6)	2.1	2.0	0.1 (7.5)	0.5	0.6	-0.1 (-12.2)
10. Sub Saharan Africa	11.4	11.8	-0.4 (-3.1)	0.7	1.1	-0.3 (-30.6)	8.1	9.1	-1.0 (-10.9)	1.0	1.5	-0.4 (-30.2)
11. Middle East	2.5	1.8	0.8 (44.7)	0.6	0.4	0.2 (36.8)	1.9	1.4	0.5 (37.3)	0.5	0.5	0.0 (0.2)
12. Central America	3.5	3.2	0.3 (9.6)	1.2	1.5	-0.2 (-16.5)	2.6	2.4	0.2 (8.3)	1.4	1.6	-0.2 (-12.7)
13. South America	9.8	8.6	1.1 (12.8)	0.6	0.8	-0.2 (-23.4)	7.3	6.8	0.5 (7.0)	0.6	0.8	-0.2 (-27.9)
14. RBU	4.1	4.7	-0.6 (-12.4)	0.3	0.3	-0.1 (-17.4)	4.3	4.9	-0.6 (-12.6)	0.8	0.7	0.1 (20.9)
15. Central Asia	1.1	1.1	0.0 (4.1)	0.0	0.0	0.0 (24.5)	1.1	1.2	-0.1 (-5.1)	0.1	0.1	0.0 (0)
17. Antarctic	0.1	0.1	0.0 (-17.5)	0.0	0.0	0.0 (0)	0.2	0.2	0.0 (-10.3)	0.0	0.0	0.0 (0)
Continental	92.9	81.1	11.8 (14.5)	13.3	15.5	-2.2 (-14.1)	73.7	64.9	8.8 (13.5)	16.8	17.9	-1.1 (-6.1)
2. Ocean	8.5	8.4	0.0 (0.2)				22.8	23.5	-0.7 (-2.9)			
1. World Total	101.3	89.6	11.8 (13.1)	13.3	15.5	-2.2 (-14.1)	96.5	88.4	8.1 (9.2)	16.8	17.9	-1.1 (-6.1)

Continue Table 5.

	NO_X emission		NO_y deposition		NH_3 emission		NH_X deposition	
	Non-coastal	Coastal	Non-coastal	Coastal	Non-coastal	Coastal	Non-coastal	Coastal
	Δ	Δ	Δ	Δ	Δ	Δ	Δ	Δ
3. North America	-0.1	-0.1	-0.4	-0.1	0.1	0.0	0.1	0.0
4. Europe	-0.4	-0.5	-0.3	-0.3	-0.6	-0.4	-0.4	-0.3
5. South Asia	2.4	0.0	2.1	0.2	3.0	-0.2	3.3	-0.1
6. East Asia	5.3	0.0	4.5	0.8	-1.6	-0.2	-1.3	-0.2
7. Southeast Asia	1.1	0.1	0.7	0.1	1.0	-0.1	1.1	-0.2
8. Australia	0.2	0.0	-0.1	0.0	-0.3	-0.1	-0.2	-0.2
9 North Africa	0.6	0.1	0.3	0.0	-0.2	0.0	-0.1	-0.1
10. Sub Saharan Africa	1.1	-0.1	0.3	-0.1	-1.5	-0.2	-1.3	-0.4
11 Middle East	0.9	0.2	0.6	0.1	-0.1	0.0	-0.1	-0.1
12. Central America	0.6	0.0	0.2	0.0	-0.3	-0.2	0.0	-0.2
13. South America	1.5	0.0	0.7	0.0	-0.3	-0.2	-0.3	-0.2
14. RBU	0.1	0.0	0.1	0.2	-0.7	-0.1	-0.7	0.0
15. Central Asia	0.2	0.0	0.1	0.0	-0.1	0.0	-0.1	0.0
17. Antarctic	0.0	0.0	0.0	0.0	0.0	0.0	-0.1	0.0
Continental	13.5	-0.4	8.9	0.9	-1.7	-1.8	-0.1	-2.0
2. Ocean	0.7		1.7		-0.7		-2.4	
1. World Total	14.2	-0.4	10.7	0.9	-2.4	-1.8	-2.6	-2.0